LBL-9130

LECTURE 1

EXPERIMENTAL EVIDENCE FOR COLLECTIVE AND THERMAL FEATURES IN HEAVY ION REACTIONS

LECTURE 2

EQUILIBRIUM STATISTICAL TREATMENT OF ANGULAR MOMENTA ASSOCIATED WITH COLLECTIVE MODES IN FISSION AND HEAVY-ION REACTIONS

Luciano G. Moretto

Lawrence Berkeley Laboratory
University of California
Berkeley, California 94720

NOTICE

This report was prepared as an account of work sponsored by the United States Government. Neither the United States nor the United States Department of Energy, nor any of their employees, nor any of their contractors, subcontractors, or their employees, makes any warranty, express or implied, or assumes any legal liability or responsibility for the accuracy, completeness or usefulness of any information, apparatus, product or process disclosed, or represents that its use would not infringe privately owned rights.

DISTRIBUTION OF THIS DOCUMENT IS UNLIMITED

LBL-9130

LECTURE 1

EXPERIMENTAL EVIDENCE FOR COLLECTIVE AND THERMAL FEATURES IN HEAVY ION REACTIONS

Luciano G. Moretto

Lawrence Berkeley Laboratory
University of California
Berkeley, California 94720

ABSTRACT

The set of degrees of freedom playing a relevant role in deep inelastic processes is discussed. General considerations concerning the dynamical regimes prevailing during the nucleus-nucleus interaction lead to interesting conclusions regarding classical and quantal features as well as to the applicability of transport theories. The damping associated with the relative distance coordinate is considered and the evidence for thermal equilibrium between fragments is presented. The role of the E1 mode and of all the other odd isovector modes on the charge distribution at fixed mass asymmetry is discussed and the possible evidence for quantal fluctuations is analyzed. The mass asymmetry degree of freedom is considered in terms of the experimental mass distributions. The origin of the two components, deep inelastic and fusion-fission is explained in terms of different dynamical regimes leading to greatly different interaction times. The rotational degrees of freedom are discussed in terms of γ-ray multiplicities and sequential fission. The problem of angular momentum fractionation along the mass asymmetry coordinate is considered and the depolarization and misalignment of the fragment spins are discussed.

Introduction

All the newcomers in a new environment are in need of an identity and strive to search for their "roots." Also the practitioners in the field of deep inelastic heavy ion processes seem to want or need an identify of their own, especially when confronted with the stern establishment of the nuclear spectroscopists.

Our own natural roots go back to the grand days of fission which, in many ways, is the process in which all the present themes of interest are represented at least in germ. So this is our root and our legacy.

Our own identity finds its focus in the wealth of new degrees of freedom associated with both fission and heavy ion reactions.

Fission first indicated the great variety of large scale collective motions which can be present in a nuclear fluid. However, fission is not an easy reaction to work with. The initial conditions for all the collective motions are left at the whim of statistical fluctuations in the compound nucleus. This fundamental inability to choose the initial conditions at our own convenience was the major difficulty that faced the searchers in this field and prevented a substantial development in our understanding for a very long time.

The advent of heavy ion reactions removed this difficulty to a very great extent. While essentially the same degrees of freedom are called into play, now we have control on the entrance channel kinetic energy, on the mass asymmetry, on the target and projectile neutron-to-proton ratios.

This new freedom has generated an exciting and varied phenomenology, which can indeed be considered the new challenge in nuclear physics.

An understanding of all this new physics can occur at various levels. Phenomenological models have taken, as expected, the lead in interpreting the new data. However this new field not only needs an identity which after all was not difficult to discover. Most of all it now needs to integrate with the conservative sectors of nuclear physics. Phenomenology may not be enough and should not be enough.

From this the microscopic quest is born. We want to cast the new theories in the framework of the old well understood spectroscopy. And, to be sure, we are now witnessing attempts to explain the new physics in terms of the shell model, or even in terms of nucleon-nucleon interaction like in the TDHF model. The role of the giant resonances in deep inelastic processes is prompting attempts to explain energy and angular momentum transfer with the same language used in the interpretation of the collective strength functions.

Admittedly we are very much at the beginning of this endeavor. Which means that the privilege of carrying this project to a good end may be ours indeed.

An Open List of "Relevant" Degree of Freedom

As pointed out before, a wealth of new degrees of freedom has substantially enriched the nuclear landscape with the advent of heavy ion reactions.[1] While it may be useful to list these degrees of freedom, we may not be able to define them uniquely. Some of them are essential to the characterization of the reaction, like the separation coordinate, and are directly connected with physical observables. Others are perhaps less essential and in fact may not be related to a physical

observable in any straightforward way. High multipole modes, isoscalar and isovector as well, are part of such a class. Even from a theoretical standpoint these modes become less defined as their multipolarity increases in view, for instance, of the surface diffuseness. A pragmatic position has frequently characterized many attempts to describe these modes. Only those modes which are directly called into cause by the experimental observation should be taken into consideration. On the other hand, an a priori judgement on the relevance of a given mode occasionally has led to experiments which have substantiated the original expectations.

Consequently, without introducing any specific model, let us make a list of those degrees of freedom which have had the chance of proving themselves already, and also of those which, in our judgement, may play an important role in the future.

(a) The fragment relative distance is well defined in the exit channel but may, or may not, be clearly defined for the intermediate complex. The evolution in shape expected to occur from compound nucleus to fission illustrates how the two fragments progressively gain their identity. This degree of freedom is well documented experimentally in terms of the asymptotic kinetic energy.

(b) The neck degree of freedom is, in principle, of dramatic importance. Together with the fragment relative distance one could conceivably construct a simple but non-trivial model to describe heavy ion collisions. Unfortunately, its relevance spreads over many observables and, so far, no clear cut experiment has characterized it.

(c) The mass asymmetry is a beautifully documented degree of freedom. The great variety of mass distributions observed experimentally have made it one of the pet degrees of freedom of this field.

(d) The fragment neutron to proton ratios are now under intense study. The distribution of charge at fixed mass asymmetry has a strong and direct connection with the E1 mode, which may be studied now in a variety of new situations.

(e) The rotational degrees of freedom are surfacing in many unexpected ways. Beside their obvious role in determining the angular distribution, they appear to affect the alignment of the fragment spin in a substantial way. Bending, twisting, wriggling, and tilting, while may not appear to belong to this class, do in fact bear angular momentum and may be worth considering here.

(f) The (many) fragment deformation coordinates may play a role in the dissipation of energy and may well be responsible for part of the fluctuations in the relaxed peak. Symmetric and asymmetric stretching could be quite relevant in this respect.

(f) Higher multipole isovector modes are conceivably important in controlling the neutron-to-proton ratio of the fragments. Very little attention has been dedicated to them so far.

(g) Thermodynamic degrees of freedom appear to play a substantial role in view of the large degree of relaxation observed in these reactions. Temperature gradients may be important and certainly the difference in temperature between the two fragments appears to be quite relevant.

Characterization of the Dynamical Regimes

After the attempt of listing the degrees of freedom, one should try to infer theoretically, or determine experimentally, what kind of dynamical regime should prevail. One of the first questions is whether a quantum or a classical regime applies.

As a statement of principle, all of these systems are quantum mechanical because we are dealing with highly degenerate Fermi fluids. This does not mean that semiclassical or altogether classical approaches may not be applicable for specific collective modes.

For instance the rotational modes may well be treated classically in so far as $I \gg \hbar$. Yet the moments of inertia will almost surely be controlled by quantal features. Even the rigid limit is dictated by the Pauli principle.

The treatment of low multipole vibrations depends upon the sharpness of their strength function. The presence of sharp peaks dictates, at least at low temperatures, a quantal treatment.[2] On the other hand, if the strength function becomes very broad, the mode cannot be properly quantized, since we lose the ability to define its kinetic energy, or its inertia (classically the mode is overdamped). In this case the mode is not a dynamical variable any longer, and can be treated as a parameter characterized by the potential energy alone. Its distribution could be, for instance, a classical Boltzmann distribution.[3]

Even within the classical limit it is not obvious which regime should apply. If one deals with large heat sinks a Lagrangian formulation of the problem should be adequate.[4] The three relevant physical quantities are

V the potential energy

$\mathcal{J}$ the inertia

R the Rayleigh dissipation function

Two regimes can immediately be identified.

If $\mathcal{J} \gg R$ the system is controlled by the inertia (underdamped).

If $\mathcal{J} \ll R$ the system is controlled by the viscosity (overdamped).

On the other hand, if the heat sinks are sufficiently small to allow the temperature to increase to values comparable with the relevant kinetic energies, fluctuations become relevant and may in fact dominate the whole picture. Diffusion is then the prevailing regime and should be described in terms of transport equations.[5,6]

Damping of the Relative Motion and the Energy Thermalization

Although the high degree of inelasticity is certainly the oldest and most venerable feature of heavy ion reactions, the most recent studies in this line present a variety of extraordinary and intriguing features which challenge our attempts to a coherent interpretation.

The degree of relaxation varies greatly from reaction to reaction, and wide ranges of Q values, extending from zero to the Coulomb barrier are frequently observed in a single reaction[7] (Fig. 1). Estimates of the relaxation time can be obtained by various means. Despite the optimism of some authors, empirical attempts to define a time scale may have uncertainties of a factor of few. Nonetheless, for purposes of orientation, the figure of $\tau_E \simeq 3 \times 10^{-22}$ sec is certainly representative of the relaxation time. This is also to be taken as an estimate of typical interaction times.

The dissipated energy is recovered to a very great extent in the evaporation from the excited fragments. It is quite remarkable that such an extensive relaxation prevails even at very high bombarding energies. For instance, in the reaction $^{63}Cu + ^{20}Ne$ at 158,252 and 343 MeV[8] the charge loss of the two fragments near symmetry was determined as a function of exit channel kinetic energy by measuring the Z of both fragments in coincidence. The missing charge dramatically increases with bombarding energy and depends linearly upon excitation energy, which can be estimated from kinematics (Fig. 2). The slope is ~25 MeV/charge. Since the total mass loss is about twice the evaporated charge, one obtains an average energy loss per particle of ~12.5 MeV which one would expect from evaporation. This indicates that, even at the highest bombarding energy the near symmetric fragments are very close to complete thermalization.

Thus very large amounts of energy appear to be dissipated in a very short time, a time so short in fact to be uncomfortably close to a single particle period (~10^{-22} sec for $\hbar\omega$ = 5 MeV). A variety of mechanisms which could be responsible for the energy dissipation in the available time has been proposed, ranging from giant mode excitation to particle transfer. The excitation of several phonons[2] and/or the random transfer of several particles (nucleons?)[9] could provide a viable <u>dynamical</u> explanation to the observed energy loss. Neither of these fast mechanisms is at variance with the ultimate fate of the excitation energy which is spent in evaporation, since thermalization could conceivably occur leisurely inside each fragment on a time scale that needs not be comparable with the interaction

time. Unfortunately a catch is found in a remarkable experimental observation. The energy appears to be divided between the two fragments proportional to their mass. In a study performed on the reaction Ag + 340 MeV ^{40}Ar,[10] the simultaneous detection of both fragments, together with the measurement of both kinetic energies, both angles and the Z of one fragment enabled us to deduce the preevaporation masses as well as the mean number of neutrons emitted by each fragment. These data (Fig. 3) establish that the Z dependence of the masses corresponds to the equilibration of the neutron-to-proton ratio while the two fragments are in contact (solid line). This feature will be discussed further later on. Furthermore the dependence of the mean number of neutrons on Z corresponds to a splitting of the excitation energy proportional to the masses, as verified by an evaporation calculation (dashed lines).

This latter point has been verified by direct measurement of neutrons from deep inelastic reactions.[11-13] These experiments verify that the energy is indeed split according to the masses (Fig. 4) and that the neutron spectra of the two fragments have the same temperature (Fig. 5). More outstanding is the fact that such an energy partition according to masses is not only observed for completely relaxed events, as in the experiment described above, but <u>also for the whole range of Q values, up to very small energy losses</u> (Fig. 6).

The simplest hypothesis which can explain all these facts is that the thermalization of the energy is so fast that it occurs on a time scale shorter (and presumably much shorter) than the interaction time, thus allowing the fragments to be in thermal equilibrium at all times during their interaction.

The problem of the statistical energy partition between the two fragments is straightforward.

The excitation energy distribution between two fragments sharing an amount of energy E is

$$P(x)\ dx \propto \rho_1(x)\ \rho_2(E-x)\ dx$$

where ρ_1, ρ_2 are the level densities of each fragment. At equilibrium one has

$$\frac{d \ln P(x)}{dx} = \frac{d \ln \rho_1(x)}{dx} + \frac{d \ln \rho_2(E-x)}{dx} = 0 = \frac{1}{T_1} - \frac{1}{T_2}$$

where T_1 and T_2 are the fragment temperatures.

The equality of the intensive quantity T implies the proportionality to mass of the extensive quantity x:

$$\frac{x}{E - x} = \frac{A_1}{A_2}$$

One could argue that, perhaps, the very dynamical process responsible for the energy dissipation may distribute the excitation energy just proportionally to the masses, thus obviating the necessity of requiring thermal equilibrium. This would be quite peculiar and it is certainly not the case if the energy is transfered by mass transfer. In fact, for this model the excitation energy ratio is

$$\frac{E_2}{E_1} \simeq 1 + \Delta\ \frac{M_2 - M_1}{M_1 M_2}$$

where M_1, M_2 are the masses of the two fragments and Δ is the mass involved in each elementary transfer (a nucleon). In other words,

to a great degree of accuracy this model predicts the same excitation energy for both fragments irrespective of their mass ratio.

Still it would seem worthwhile to further check if the two fragments are indeed in thermal equilibrium, in view of the dramatic relevance of this result on the relaxation time. An immediate and direct way is to check the excitation energy fluctuation between the two fragments. We can estimate this quantity by calculating the second moment of the kinetic energy distribution

$$P(x) \propto e^{-\frac{(x - x_0)^2}{2\sigma^2}}$$

$$\frac{\partial^2 \ln P(x)}{\partial x^2} = -1/\sigma_2 = \frac{\partial^2 \ln \rho_1(x)}{\partial x^2} + \frac{\partial^2 \ln \rho_2(E-x)}{\partial x^2}$$

$$= \left.\frac{\partial_1/T_1}{\partial x_1}\right|_{T_1=T} + \left.\frac{\partial_1/T_2}{\partial x_2}\right|_{T_2=T} = -\frac{1}{T^2}\left(\frac{1}{C_{V1}} + \frac{1}{C_{V2}}\right)$$

from which

$$\sigma^2 = T^2 \frac{C_{V_1} C_{V_2}}{C_{V_1} + C_{V_2}}$$

where C_{V1}, C_{V2} are the heat capacities of the two fragments. For a Fermi gas system one obtains

$$C_V = 2aT$$

and

$$\sigma^2 = 2T^3 \frac{a_1 a_2}{a_1 + a_2}$$

where a_1, a_2 are the level density parameters of the two nuclei.

Notice that the fluctuation is at a maximum when the fragments are equal, so, if $a_1 = a_2 = a$ we have

$$\sigma^2 = aT^3$$

and

$$\frac{\sigma}{x_0} = \left(\frac{2}{aE}\right)^{\frac{1}{4}}$$

where E is the dissipated energy. For E = 100 MeV and A_{total} = 200 one obtains (a = A/8).

x_0 = 50 MeV , σ = 10 MeV

or an easily measurable effect.

What one needs to measure is, for instance, the correlated number of neutrons emitted by each fragment for events with the same Q value. Unfortunatly the covariance analysis of these data has not been performed as yet.

If one can indeed rely on the fact that the two fragments are in thermal equilibrium even at the smallest Q values and thus for the smallest interaction times, a treatment of the energy loss in terms of a simple transport equation, like the Master Equation or the Fokker-Planck equation would definitely be warranted.[6]

The Neutron-To-Proton Ratio and the Giant Isovector Resonances

In heavy ion collision the neutron-to-proton ratio of the two fragments seems to undergo equilibration rather quickly ($\tau_{N/Z} \simeq 10^{-22}$ sec). The most probable value closely corresponds to that obtained by requiring that the potential energy be minimized with respect to the Z of one of the two fragments in contact, at fixed mass asymmetry. This implies that the degree of freedom controlling the neutron-to-proton ratio relaxes faster than the mass asymmetry degree of freedom.

We have pointed out before that the neutron-to-proton ratio degree of freedom can be identified with the E1 giant mode, and more precisely with the low energy component of the quadrupole-split giant E1 resonance in prolate nuclei. This component corresponds to the sloshing back and forth of the neutrons against the protons along the deformation axis, and clearly controls the charge distribution of the fragments forming the intermediate complex. One should of course keep in mind (and we shall return to this point later) that all the odd isovector modes potentially can contribute to the determination of the fragment neutron-to-proton ratio as well.

Coming back to the E1 mode, it is clear that from the equilibrium value of the neutron-to-proton ratio we learn only about the potential energy term of the collective Hamiltonian. A way to obtain information on the total collective Hamiltonian for all the odd isovector modes, hopefully dominated by the E1 mode, is to look at the distribution of neutron-to-proton ratios at fixed mass symmetry, because this distribution can be related to the modulus square of the collective wave function.

Let us assume that the E1 mode is fully quantized.[3] We can try to estimate the phonon energy from the expression

$$\hbar\omega = 94/d \text{ MeV} \quad ,$$

where d is the semimajor axis of the intermediate complex. This expression assumes that the neutron-to-proton ratio is frozen when the neck between the two fragments is quite large (remember that this expression is used to evaluate the E1 quadrupole splitting in deformed nuclei). If equilibrium were to be retained for smaller neck sizes, the relevant phonon energy could be substantially lower.

For a great deal of target-projectile combination, the phonon energy is in the range 6-10 MeV, much greater than the typical temperature of 1-2 MeV. Since $\hbar\omega/T \gg 1$, the collective E1 mode should be almost completely in its ground state. Therefore the Z distribution at fixed mass asymmetry should be given by the modulus square of the ground state wave function and the second moment of the distribution should be:

$$\sigma^2 = \frac{\hbar\omega}{2c}$$

where c is the stiffness constant defined by:

$$V_{(E1)} = \frac{c}{2} (Z - Z_0)^2$$

and can be easily determined from the liquid drop model. The expected values of the charge variance are in the range: $\sigma^2 \simeq 0.6,\ 1.0\ e^2$ Before turning to the experimental results, it is worth appreciating that, through the measurement of the change dispersion, one can

potentially learn about the E1 mode in unusually deformed nuclei at large excitation energies.[3] Both of these situations are not accessible to the standard methods applied to the study of the giant resonance namely photoexcitation and photodecay. The experimental situation is somewhat perplexing. A large body of data ranging from Ar induced to Xe induced reactions yields very small variances, consistent with the relation

$$\sigma_Z^2 = \frac{T}{c}$$

as if the collective mode were not quantized at all and the distribution were a classical Boltzmann distribution:[14]

$$P(Z) = e^{-\frac{1}{2} c \frac{(Z-Z_0)^2}{T}}$$

See for instance Fig. 7. The outstanding problem is then to understand why the distribution in Z is classical rather than quantal, as one would expect.

The explanation may reside[3] in the damping of the collective E1 mode. In photoexcitation, the giant resonance is mainly a 1p,1h state and presumably owes its width to the coupling into the 2p,2h states. In the case of 280 MeV Ar + Ni,[15] at relatively high excitation energy (60 MeV), the collective mode is an (np,nh) state which may couple into (n + 1p, n + 1h) or (np,nh), or again, ((n - 1)p, (n - 1)h) states. The resulting damping is energy-dependent and due mainly to the increasing density of the doorway states with increasing energy. It is interesting to see the consequence of this coupling to the Z

distribution. Following Bohr and Mottelson with a simple generalization, we can describe the coupling of the collective state $|a\rangle$ to the doorway states $|\alpha\rangle$. The exact state $|i\rangle$ is given by

$$|i\rangle = |a\rangle + \frac{P}{E_i - H_0 - V} V|a\rangle$$

where $P = \sum_\alpha |\alpha\rangle\langle\alpha|$, H_0 is the unperturbed Hamiltonian, and V is the perturbation.

The relevant charge distribution is given by $P_i(z) = \int dx|\psi_i(z,x)|^2$, where $\psi_i(z,x) = \langle z,x|i\rangle$, and x denotes all other variables which must be projected out. In order to compare theory with experiment we have to consider the average of the distribution over an energy interval around E_i. We can write

$$P_i(z)_{ave} = \int dx[|\{\psi_i(z,x)\}_{ave}|^2 + \{|\psi_1^f\ (z,x)|^2\}_{ave}]$$

with $\psi_i^f = \psi_i - \{\psi_i\}_{ave}$ the "fluctuating" wave function. The fluctuating part can be shown to be responsible for the <u>broadening</u> of the distribution. It leads to a statistical distribution for Z. We want to show that the first term can lead to a <u>narrowing</u> of the distribution. For this purpose we have to consider the averaged Green function $\{1/(E_i - H_0 - V)\}_{ave}$. This average has been considered extensively in the literature. For large systems and high excitation energies only the average diagonal matrix elements of the resolvent have to be considered and it can be shown that

$$\left\{\langle\alpha\left|\frac{P}{E_i - H_0 - V}\right|\alpha\rangle\right\}_{ave} = \frac{1}{E_i - E_\alpha - i\Gamma}$$

where Γ is the imaginary part of the "equivalent optical potential" describing the dissipation of the state $|a\rangle$ into the states $|\alpha\rangle$. The amplitude of the state $|a\rangle$ contained in the average eigenstate $|i\rangle$ is given by

$$c_a(i) = \left(1 + \sum \frac{V_{\alpha a}^2}{(E_i - E_\alpha - i\Gamma)^2}\right)^{-1/2}$$

In summary, the omitting for simplicity the bracket of the average,

$$|i\rangle = c_a(i)|a\rangle + \sum_\alpha c_\alpha(i)|\alpha\rangle \quad .$$

The next step is to establish that the sum over α in the above equation is a <u>coherent</u> one, and thus the corresponding term describes a wave packet, i.e., it leads to a <u>narrowing</u> of the distribution. One can prove that if $V_{a\alpha}$ is random, the vectors $|\alpha\rangle$ contain phases which destroy the random property of $V_{a\alpha}$. Having established this point from first principles, we are entitled to use as first guess a simple-as-possible model. The average wave function associated with the charge asymmetry coordinate can be written as

$$\phi_i(z) = c_a(i)\ \psi_a(z) + 1/D \fint dE_\alpha c_\alpha(i)\ \psi_\alpha(z)$$

where D is the level spacing of the available doorway states and $\psi_a(z)$ is the ground state wave function of the E1 mode:

$$\psi_a(z) = \sqrt{2\pi\hbar\omega/c}\ \exp[-cz^2/2\hbar\omega] \quad .$$

Qualitatively one sees already that, as the coupling increases, the integral in the expression for Φ_i becomes progressively dominant and,

the more states that are called into play by the strength of the coupling, the narrower $\Phi_i(z)$ becomes. As a qualitative first guess on the $\psi_\alpha(z)$ we can use the plane wave expression

$$\psi_\alpha(z) = \sqrt{2\pi\hbar\omega/c}\ \exp\left(iz\sqrt{c/2\hbar\omega}\sqrt{E_\alpha/D_1}\right)$$

where the plane waves are normalized to unity in a z box of volume corresponding to that of the harmonic oscillator. By taking $\Gamma = \hbar(\lambda^+ + \lambda^0 + \lambda^-)$, where λ^+, λ^0, λ^- are the transition probabilities from (np,nh) to (n+1p, n+1h), (np,nh) and (n-1p, n-1h) states, respectively, the integral in the expression for $\Phi_i(z)$ can be evaluated and gives as a result

$$2\ \exp\left(-iz\sqrt{c/2\hbar\omega}\sqrt{1/D_1}\sqrt{E_i - i\Gamma}\right) .$$

The second moment of the z distribution, σ_z^2, can then be obtained from the z distributions given by the modulus square of Φ_i.

The calculated second moment of the distribution σ_z^2 vs excitation energy is shown in Fig. 8. The narrowing of the distribution with increasing energy is quite evident. Since this calculation does not include thermal fluctuations, they are introduced in the simplest way,

$$\sigma_z^2 = \sigma_{z,Q}^2 + \sigma_{z,T}^2$$

where the labels Q and T stand for quantal and thermal.

On the other hand a recent experiment on Mo + Kr^{16} shows variances $\sigma^2 \simeq 1.0\ e^2$, which are consistent with purely quantal rather than thermal fluctuation (see Fig. 9). The apparent contradiction between these two sets of data is mystifying and an exciting mystery. One

obvious difference is that the "thermal systems" are highly asymmetric, while the "quantal system" is nearly symmetric. However it is not clear how to relate this aspect to the different behavior of the two systems.

On the theoretical side, one of the limitations of the model used so far is the inclusion of the lowest odd isovector mode only. One should consider in detail the effect of the zero point motion associated with all the other odd isovector modes.

But, perhaps the answer still lies in additional experiments to confirm or disprove the present experimental situation.

The Mass Asymmetry Mode and the Charge or Mass Distributions

An inspection of the now abundant data on the mass or charge distributions associated with heavy ion reactions show the presence of two components[1] which are usually quite distinct for values of E/B ratio larger than 1.5 and frequently merging together for $E/B < 1.5$. The first component which we call deep inelastic component is relatively narrow, concentrated around the target and projectile masses, its width varies with Q value and angle, its angular distribution is side-peaked or forward-peaked. The second component, which we call fusion-fission component, when it exists, is broad, peaked at symmetry, is associated with the most relaxed Q values and its angular distribution is symmetric about 90° and close to $1/\sin\theta$.

a) The Deep Inelastic Component

The former component has all the characteristics of a non equilibrium process and its time dependence is portrayed in many experimental features.

A comparison of the widths of the charge distributions at various angles associated with the first component leads to an estimate for the relaxation time along the mass asymmetry coordinate $\tau_A \cong 60 \times 10^{-22}$ sec. This is the largest relaxation time observed so far, much larger than the typical interaction time. A good impression about the time dependence associated with this mode can be obtained by observing the dependence of the width of the distribution upon Q value[17,18] (Fig. 10). One can easily notice how the width increases with increasingly negative Q value. Yet even at the maximum Q value, when the relative motion appears to be fully relaxed, the mass distribution is far from being equilibrated.

An even better feeling can be obtained by observing the dependence of the angular distributions upon the fragment atomic number[7] (Fig. 11). Most remarkably, while the fragments close in Z to the projectile show a side-peaked angular distribution, characteristic of very short interaction times, the fragments farther removed in Z from the projectile show a progressive weakening of the side peak, until, very far away from the projectile Z, the angular distributions become distinctly forward peaked. The evolution from side peaked to forward peaked angular distributions corresponds qualitatively to an increasing interaction time.[7] The data are thus very suggestive of a time progression in the population of the configurations with atomic numbers farther and farther removed from the projectile.

This feature, together with the rapid thermalization of kinetic energy and the large time constant of the mass asymmetry mode suggest the possibility that the mass asymmetry evolves in a Markovian fashion

towards equilibrium by maintaining a strong coupling to the heat bath provided by all the other degrees of freedom. The applicability of the Master Equation and of the Fokker-Planck equation to the time evolution of the various collective modes has been discussed in detail from a theoretical standpoint without a clear cut conclusion.[19,20] However, the success of their application to a great variety of features in heavy ion reactions is undoubtable. In particular these approaches are singularly successful when applied to the mass asymmetry degree of freedom.

If we assume that the intermediate complex has a shape close to that of two touching fragments, the asymmetry of the system can be characterized by either the mass or the charge of one of the two fragments. We further assume that the time evolution along the asymmetry coordinate is diffusive in nature and describable in terms of the Master Equation:[1,21]

$$\dot{\psi}(Z,t) = \int dZ' \; \Lambda(Z,Z') \; \psi(Z',t) - \Lambda(Z',Z) \; \psi(Z,t)$$

where $\psi(Z,t)$ and $\dot{\psi}(Z,t)$ are the populations of the configurations characterized by the atomic number Z of one of the fragments and their time derivative at time t; and $\Lambda(Z,Z')$ and $\Lambda(Z',Z)$ are the macroscopic transition probabilities.

If one writes $Z' = Z + h$ and all the quantities are expanded about Z in powers of h, one obtains to low order:

$$\psi(Z,t) = -\frac{\partial}{\partial Z}[\mu_1\psi] + \frac{1}{2}\frac{\partial^2}{\partial Z^2}[\mu_2\psi]$$

which is the well-known Fokker-Planck equation. The quantities μ_1 and μ_2 are the first and second moment of the transition probabilities

$$\mu_1 = \int h\Lambda(Z,h)\, dh \quad ; \quad \mu_2 = \int h^2\Lambda(Z,h)\, dh \quad .$$

The Fokker-Planck equation has simple analytical solutions when μ_1, μ_2 are constants and for the initial condition $\psi(Z,0) = \delta(Z - Z_0)$:

$$\psi(Z,t) = (2\pi\mu_2 t)^{-1/2} \exp\left\{-[Z - (Z_0 + \mu_1 t)]^2 / 2\mu_2 t\right\} \quad .$$

Notice that the centroid of the Gaussian moves with velocity μ_1 which can be related to the driving force $F = -V_Z'$ and to the friction coefficient K by the relation: $K = \mu_1 F$.

When the force is harmonic,

$$V_Z = c/2\ (Z - Z_{sym})^2 = 1/2\ ch^2 \quad ,$$

an analytic solution is also available

$$\psi(h,t) = c^{1/2}\left[2\pi T\left(1 - \exp - \frac{2ct}{K}\right)^{-1/2}\right]$$

$$\times \quad \exp\left\{-\frac{c[h - h_0 \exp - ct/K]^2}{2T(1 - \exp - 2ct/K)}\right\}$$

where we have made use of the Einstein relation $\mu_1/\mu_2 = -V_Z'/2T$ and T is the temperature.

The difficulties arise in the choice of the transition probabilities. Assuming that no doorway states play any special role, the golden rule implies that:

$$\Lambda(Z,Z') = \lambda(Z,Z')\rho_Z$$

where $\lambda(Z,Z')$ is the microscopic transition probability and ρ_Z the level density of the configuration associated with Z. On general

grounds one could guess the form

$$\Lambda(Z,Z') = Kf \frac{\rho_Z}{\sqrt{\rho_Z \rho_{Z'}}} \quad ; \text{ or} \quad \Lambda(Z,Z') = 2Kf \frac{\rho_Z}{\rho_Z + \rho_{Z'}}$$

where Kf is the rate-controlling factor, related to the particle transfer rate. The transition probabilities can be written as:

$$\Lambda(Z,h) = Kf \exp(-V_Z' h/2T)$$

in the former case and

$$\Lambda(Z,h) = Kf \frac{\exp(-V_z' h/2T)}{\exp(-V_z' h/2T) + \exp(V_z' h/2T)}$$

in the latter case.

Assuming that only adjacent configurations are coupled by the transfer of uncorrelated particles, one obtains

$$\mu_1 = -2\, Kf \sinh V_Z'/2T \cong -\frac{Kf\, V_Z'}{T}$$

$$\mu_2 = 2\, KF \cosh V_Z'/2T \cong 2\, Kf$$

in the former case or

$$\mu_1 = -2\, Kf \tanh V_Z'/2T \cong \frac{-Kf\, V_Z'}{T}$$

$$\mu_2 = 2\, Kf$$

in the latter case.

In both cases the Einstein relation is approximately satisfied. Alternatively, if particle transfer is specifically assumed to be the

doorway state,[21] one can consider the transfer of a particle between two fragments with chemical potential differing by an energy $a = V'h$. The transition probability is then:

$$\Lambda(Z,h) = Kf \int \frac{d\varepsilon}{1 + \exp(\varepsilon - a)/T} \left(1 - \frac{1}{1 + \exp \varepsilon/T}\right) = Kf \frac{V_Z' h}{1 - \exp(-V_Z' h/T)}$$

From this we obtain

$$\mu_1 = -Kf\ V_Z' \quad ; \quad \mu_2 = Kf\ V_Z' \coth V_Z'/2T \cong 2KfT$$

Again the Einstein relation is approximately satisfied. Randrup[22], on the basis of the one body model calculates

$$Kf = 2\pi\ n_0 \bar{R}\ b\ X(\zeta)/T_F$$

where n_0 is the particle flux in nuclear matter of saturation density,

$$\bar{R} = \frac{C_1 C_2}{C_1 + C_2}$$

is the reduced radius in terms of the central radii C of the two fragments: b is the skin thickness; and $X(\zeta)$ is a universal function depending upon the separation between the sharp surfaces of the two fragment in units of the surface thickness; T_F is the Fermi energy. This approach neatly factors out the geometrical features of the problem.

The necessary potential energy can be written as:

$$V(Z,\ell) = V_{LD}(Z) + V_{LD}(Z_T - Z) + V_{Prox}(Z,\ell) + V_{Coul} + V_{Rot}$$

The first two terms are the liquid drop masses of the two fragment. The third is the nucleus-nucleus potential (for example one can use

the proximity potential), the fourth and the fifth are the Coulomb and the rotational energy.

The total potential V depends on the fissionability of the system X, on the angular momentum ℓ and on the distance between fragment centers D.

A diffusion calculation is now possible if the distance between the two fragments and the interaction time are defined. These quantities clearly depend upon the detailed features of relative motion and of the angular degrees of freedom. Simple ansatz for the average fragment distance and interaction times as a function of energy and angular momentum lead to rather satisfactory results[21] both for the mass distributions (Fig. 12) and for the angular distributions for individual fragments (Fig. 13). In particular, one can notice how elegantly the side peaking is reproduced in the vicinity of the projectile and how the forward peaking progressively dominates as one moves away from the projectile.

If the one-body dissipation is employed in treating the dynamical part of the problem, one obtains a complete formalism that should consistently reproduce the energy dissipation as well as the charge and mass distribution as a function of angle. Calculations along this line are in progress. It should be mentioned here that brave attempts have been made to deduce the Fokker-Planck coefficients directly from the experimental data.[24] This method is based upon the determination of the charge distribution widths for a sequence of contiguous Q value bins. It is claimed that with this procedure it is possible to assign an average angular momentum to each Q value bin. It is then possible to correlate angular momentum to energy loss and to the charge distribution width. While these correlations are

of definite qualitative value, the quantitative aspects of the method are very uncertain and severe systematic errors are almost inevitable.[33] At the moment, any conclusion on the validity of various models, in particular of the one body dissipation based upon the correlation between energy loss and charge distribution width is perhaps premature.

b) The Fusion-Fission Component

This component, characterized by relaxed kinetic energies, by symmetric mass distributions peaked at symmetry, and by angular distribution symmetric about 90° has been frequently confused with compound nucleus fission due to the apparent equilibration along the mass asymmetry coordinate and to the long interaction time shown by the angular distributions.[25-28]

Evidence that one may not be dealing with true compound nucleus fission, surfaces when one tries to fit the excitation function of this component in terms of a fission-evaporation competition model.[28] The excitation function apparently can be fitted only at the cost of sacrificing our confidence in the liquid drop fission barriers and their angular momentum dependence. A reduction of the liquid drop barriers by as much as 40% is required to fit the data.[28]

This seems to indicate that "fission" does not actually compete with the other evaporation channels, thus showing that no compound nucleus is formed. Most likely a metastable long-lived intermediate is formed in the neighborhood of the barrier, which has time to equilibrate along the mass asymmetry coordinate, but which has either no time nor inclination to contract into a compound nucleus, but decays into two fragments directly.

What happens may in fact be a rather complicated story and we are going to explore only one aspect of it.[29] The most sophisticated models used to calculate fusion cross sections utilize radial potentials which, at suitably low angular momentum, portray a minimum or pocket. The trajectory is then calculated utilizing a suitable friction (one-body, for example). When an orbit is trapped into the pocket, the system is assumed to fuse (to form a compound nucleus?) and the associated cross section is assigned accordingly.

Yet a system in a trapped orbit is not really trapped if it has enough thermal energy to overcome the barrier as it frequently happens. In fact, it is trivial to calculate the decay width:

$$\Gamma_{out} = \frac{\int_0^{E-B} \rho_B(X)\, dx}{\frac{2\pi}{h} \iint \rho_P\left(E - \frac{p^2}{2m} - \frac{ar^2}{2}\right) \quad dpdr}$$

where E is the total energy above the minimum; B is the height of the barrier seen from the pocket; E-B-X is the kinetic energy over the barrier, controlled by thermal fluctuations; ρ_B is the level density over the barrier; p is the radial momentum inside the pocket, also arising from thermal fluctuations; a is the second derivative of the potential at the minimum and ρ_P is the level density of the system inside the pocket. Both in ρ_B and ρ_P the radial coordinate is not included since it is treated explicitly.

Both integrals can be evaluated approximately to yield:

$$\Gamma_{out} = \hbar\omega\, e^{-B/T}$$

where $\hbar\omega$ is the phonon energy associated with the oscillations inside the pocket and T is the temperature of the system. From the above equation we can calculate the decay lifetime τ_{out}

$$\tau_{out} = \tau_{osc} \exp B/T$$

where τ_{osc} is the oscillation period inside the pocket. It is apparent that the range of ℓ waves associated with values of $B/T \leqslant 1$ have an excellent chance to hop out of the pocket.

Of course, while the system tries to decide whether to hop out or not (and it may take some time), several things can happen. On the one hand the system may drift along the mass asymmetry coordinate and attain local equilibrium. On the other it may take an alternate route towards the compound nucleus configuration (other than the mass asymmetry coordinate). In the meanwhile the system is rotating.

An extreme simplification is to assume that, if an orbit is not trapped, the system will split apart after some amount of mass diffusion, thus giving rise to a deep inelastic event. If, on the other hand, the orbit is trapped, the system will equilibrate along the mass asymmetry coordinate and decay, thus giving rise to a Z distribution of the form:

$$P(Z) \propto \sum (2\ell + 1) \frac{\rho(Z,\ell)}{\sum_{Z'} \rho(Z',\ell)}$$

where $\rho(Z,\ell)$ are the level densities at a given asymmetry Z and angular momentum ℓ.

An example of the calculation[29] is shown in Fig. 14 where one can see both the deep inelastic peak and the fusion fission peak equally well fitted.

The Relaxation of the Rotational Degrees of Freedom

a) The Equilibrium Limit

The relaxation of the rotational degrees of freedom can be best appreciated if one considers two spheres which, during the collision, interact through conservative and dissipative forces. The torques so generated induce a rotation in the fragments at the expense of the orbital angular momentum. The secular equilibrium, which is eventually attained if the two spheres interact for a sufficiently long time, correspond to rigid rotation, namely to the regime characterized by a matching of the orbital and intrinsic angular velocities. The angular momentum partition between orbital and intrinsic angular momentum is then fixed, and depends upon the mass ratio of the two fragments as:

$$\frac{I_{int}}{I_{tot}} = \frac{\mathcal{J}_1 + \mathcal{J}_2}{\mu d^2 + \mathcal{J}_1 + \mathcal{J}_2}$$

where I_{int}, I_{tot} are the intrinsic and total angular momenta; μ is the reduced mass; d the distance between centers; $\mathcal{J}_1, \mathcal{J}_2$ are the two fragments momenta of inertia. This ratio is 2/7 at symmetry (two touching equal spheres) and increases with increasing mass asymmetry until it reaches 1 for the maximum asymmetry in which one of the two spheres is vanishingly small.

In literature one finds an intermediate limit often quoted: the "rolling limit." This very artificial limit corresponds to the

assumption that only "sliding friction" is acting, until the two touching surfaces do not slide any longer, and no "rolling friction" is acting on the system. This limit requires the matching of peripheral velocities and, for two touching spheres, predicts an angular momentum ratio:

$$\frac{I_{int}}{I_{tot}} = \frac{2}{7}$$

irrespective of the asymmetry. The lack of practical significance for this limit is seen in the general case in which both "sliding" and "rolling friction" are simultaneously active. Under these circumstances the rolling limit is never attained.

The rigid rotation limit is visibly attained in certain reactions where the deep inelastic process is associated with a rather narrow angular momentum window. Such a limit is demonstrated by the rising γ-ray multiplicity with increasing mass or charge asymmetry[30,31] (Fig. 15). (The γ-ray multiplicity is taken here as a measure of the intrinsic angular momentum. Under optimal circumstances, the greatest amount of the angular momentum is removed by stretched E2 γ-decay. Additional γ-rays, mainly E1 decays, occur through statistical emission. A relation frequently used and occasionally tested is $M_\gamma = I/2 + a$, where a is a number between 2 and 4.)

b) <u>The Relation Between Angular Momentum Transfer and Energy Dissipation</u>

Two extreme models for the process of energy dissipation have been proposed, the excitation of giant modes on one hand, and the nucleon transfer on the other. Both of these models predict large

energy losses, in approximate agreement with experimental observations. There has been great hope, and there is still some, that the correlation between energy loss and angular momentum transfer predicted by the two models is so different that the experimental data could decide in favor of either one, or point to combination of the two mechanisms (Fig. 16a).

Unfortunately, it is easy to show that the problem is not very clear indeed. The kinetic energy E above the Coulomb barrier can be split into radial and tangential energies:

$$E = E_{rad} + E_{tang} = E_{rad} + \frac{\ell^2}{2\mu r^2} = \frac{\ell_{max}^2}{2\mu r^2}$$

where ℓ is the entrance channel angular momentum, μ is the reduced mass and r is the sum of the fragment radii. Clearly any model trying to dissipate the tangential energy must do so by transferring some orbital angular momentum into the fragments as spin. If the shapes are forced to remain the same, the correlation between energy dissipation and the fragment spin is "almost" fixed by the conservation of angular momentum and thus "almost" model independent. ("Almost" because the angular momentum conservation fixes the vectorial sum of fragment spins and not the sum of the spin moduli). A greater flexibility is available for the radial energy. However under the best of circumstances the average radial energy is only 1/2 of the total and in more realistic circumstances may be much less. For instance if the lower part of the ℓ-waves corresponding to 1/3 of the total cross section goes into compound nucleus, or goes into a completely relaxed two body decay, then the average radial energy is only 1/3 of the total. Furthermore, since the radial energy appears to be dissipated rapidly, it follows

that very little play is left to decide between the models. In other words any model is expected to reproduce reasonably well the correlation between energy loss and angular momentum transfer in all but the regions where sizeable fluctuations are expected (see Figs. 16a,21). In view of these considerations it is not too surprising to find out that the relaxation time for the angular momentum transfer is $\tau_I \cong 3.0 \times 10^{-22}$ sec, very close to the estimate for the energy relaxation time.

c) Dependence of the γ-Ray Multiplicity Upon Mass Asymmetry

In contrast with the conclusions reached above, a study of the angular momentum transfer as a function of energy and mass asymmetry should be more useful, because the varying asymmetry is certainly associated with net mass transfer, though the total back-and-forth mass transfer may not be easy to determine experimentally. On the other hand, the dependence of the γ-ray multiplicity upon mass asymmetry is complicated by other features as well, which may be even more important.

From the relatively scant, experimental evidence, one can summarize the experimental situation as follows: (a) in the quasi-elastic region the dependence of the γ-ray multiplicity upon mass asymmetry is V-shaped,[30,32] with the minimum at the entrance channel asymmetry (Fig. 16b). (b) in the deep inelastic region the γ-ray multiplicity sometimes increase with increasing asymmetry when the deep inelastic process involves a narrow ℓ-window[30,31] (Fig. 15); it usually stays more or less constant with mass asymmetry when the deep inelastic process involves a very large ℓ-window[32] (Fig. 17).

The V-shaped dependence of the γ-ray multiplicity in the quasi-elastic region can be explained either in terms of the angular momentum

transfer associated with mass transfer or, and it may be the same thing, in view of the fact that the average energy loss increases as one moves away from the entrance channel asymmetry.

The rising γ-ray multiplicity with increasing asymmetry for narrow ℓ-windows may be directly attributed to rigid rotation.

The flat dependence of the γ-ray multiplicity vs mass asymmetry, for broad ℓ-windows does not imply that there is no rigid rotation. On the contrary, it is most likely due to angular momentum fractionation along the mass asymmetry coordinate. Since the experiments suggest that the interaction times are a decreasing function of angular momentum and the spread of the cross section along the mass asymmetry should increase with increasing interaction times, it follows that the high ℓ-waves populate configurations with asymmetries close to the injection asymmetry, while the low ℓ-waves can spread farther out to much greater asymmetries. Thus the average entrance channel angular momentum decreases as one moves away from the entrance channels asymmetry. In particular the decrease in ℓ-wave as one moves towards larger asymmetries (lower Z's) may compensate the rising trend required by the rigid rotation condition, thus generating a very weak dependence of the fragment spin and of the γ-ray multiplicity upon mass asymmetry.

d) Results of a Simple Model of the Dependence of the γ-Ray Multiplicities Upon Mass Asymmetry and Q Value

This problem is equivalent to drawing the lines of constant entrance channel angular momentum in the plane defined by the total kinetic energy and by the fragment atomic number. Empirical prescriptions[24] suggesting that such lines are horizontal lines parallel to the Z axis have not

been justified and at large negative Q values are clearly incorrect.[33] Therefore even a limited attempt at solving the problem from a theoretical standpoint is justifiable.[33]

In the limit of infinite radial friction the total kinetic energy

$$E = V_{Coul}(Z) + \frac{\hbar^2 \ell_{rel}^2(\dot{Z},\ell)}{2\mu(Z)\ d^2(Z)}$$

where ℓ_{rel} is the orbital angular momentum in the exit channel, μ is the reduced mass, d is the distance of the two fragments at scission, and Z is the atomic number of one of the two fragments. There are two limiting patterns these lines of constant entrance channel angular momentum should display, corresponding to the two extreme regimes associated with the rotational degree of freedom of the intermediate complex. In the first limiting case the reaction occurs with no transfer of angular momentum from orbital motion to intrinsic spin. In this case, the angular momentum of relative motion as a function of Z, $\ell_{rel}(Z,\ell)$ is a constant independent of Z and equal to ℓ. The curves in Fig. 18a show examples for this case assuming the shape of the complex to be two touching spheres.

In the second limiting case the complex is rotating as a rigid body at the time of scission, regardless of the impact parameter (ℓ-wave). In this case, the relative angular momentum is Z-dependent, and given by:

$$\ell_{rel}(Z,\ell) = \frac{\mu_Z d_Z^2}{\mu_Z d_Z^2 + \mathcal{J}(Z) + \mathcal{J}(Z_T - Z)}$$

where $\mathcal{J}(Z)$ is the moment of inertia of a fragment with charge Z about its own axis, and Z_T is the total charge in the composite system.

This expression can be used to calculate the lines of constant ℓ for this case. The curves in Fig. 18b show examples of this behavior for the same ℓ-waves as for the previous case.

Qualitatively, one would expect the correct curve for near grazing ℓ-waves to be intermediate between the two extremes and to look like the dotted curve in Fig. 18c. A more reliable conclusion on the qualitative and quantitative aspects of this problem can be obtained from a model calculation which we have performed.

Consistent with experiment, it is assumed that the radial kinetic energy is dissipated immediately at the interaction radius. (For the lowest ℓ-waves, the interaction times appear to be long compared to the relaxation time of the radial kinetic energy, and for the highest ℓ-waves, even though the interaction times are short, very little of the kinetic energy is in the radial coordinate). The analysis is restricted to a system of two spheres separated by an ℓ-dependent distance, $d(\ell)$, dynamically determined. We need to calculate how the orbital angular momentum (ℓ_{rel}) is transferred into the spins of the nuclei (I_1,I_2) and the functional dependence of I_1 and I_2 on the asymmetry of the complex (Z). This calculation is performed by assuming that particle transfer is responsible for energy and angular momentum transfer.

Figure 19a shows the predictions of the model of the system 1156 MeV $^{136}Xe + ^{197}Au$. Each pair of adjacent lines brackets 5% of the reaction cross section. The qualitative behavior predicted above is now very apparent. Figure 19b shows the upper portion of Fig. 19a with contours of constant cross section (as calculated by the Fokker-Planck equation)

drawn in. The horizontal lines divide the data into ten bins, 30 MeV wide. (Only every other line is shown for ease of viewing.) The lines of constant ℓ calculated by the model are chosen to coincide with the parallel lines at the Z of the projectile. Figure 20 is a plot of the ratio of the variance predicted by the present model and the variance derived from the parallel cuts. Note the large difference for the first few bins. It is exactly in this energy region that a previously mentioned discrepancy between the experimental and theoretical (one-body theory) energy loss per particle was found. The empirical analyses seemed to indicate that the experimental energy loss per particle, calculated as

$$\varepsilon = \frac{(E_{cm} - TKE_{bin})}{\sigma_Z^2 \alpha}$$

(α being the conversion factor defined by $\sigma_A^2 = \alpha\sigma_Z^2$) was between two and three times larger than the expected from a one-body dissipation mechanism. If the empirical variances are in error by as much as indicated by the present work, the discrepancy between theory and experiment disappears.

This model, which allows one to calculate the Z and Q value dependence of the intrinsic angular momentum, can be used to analyze the experimental γ-ray multiplicities. All that is needed is a transformation from angular momentum to γ-ray multiplicity. The transformation from fragment spin to γ-ray multiplicity is based upon the assumption that most of the fragment angular momentum is removed by stretched E2 decay. More specifically we use the following transformation:

$$I_1(Z_1E_k) + I_2(Z_1E_k) = 2(M_\gamma - 2a)$$

where I_1 and I_2 are the fragment spins, M_γ is the γ-ray multiplicity, and a is the mean number of statistical γ-rays emitted by each fragment. Compound nucleus studies with heavy-ion reactions indicate that $a \simeq 2 - 3.5$ depending upon the nucleus. Because of this uncertainty, caution must be exercized in comparing the absolute values of the measured and calculated multiplicities.

The kinetic energy dependence of the γ-ray multiplicities will be considered first. In Fig. 21 the γ-ray multiplicity M_γ associated with both fragments in the reactions Au, Ho, Ag + 618 MeV ^{86}Kr is plotted as a function of the total kinetic energy of each pair.[34] Both in the experiment and in the theory, the γ-ray multiplicities are integrated over all the exit channel asymmetries. The number of statistical γ-rays per fragment is taken to be three.

The plateau in the experimental multiplicities and the maximum in the calculated multiplicities corresponds to a regime very close to rigid rotation. The theoretical drop at lower kinetic energies is due to the effect of the Coulomb energy (which in the model is taken to be that of two touching spheres) and the fact that lower angular momenta, in the limit of rigidly rotating touching spheres, are associated with lower kinetic energies. The experiment does not show a drop in multiplicity as large as the theory does, because the exit channel configuration is not constrained to that of two touching spheres. Thus the deep inelastic component is spread over an energy range extending well below the Coulomb barrier. Furthermore, fluctuations in shape and fragment angular momentum may destroy the simple correlation between

kinetic energy and angular momentum predicted by the model at these low energies.

The second aspect to be analyzed is the Z-dependence of M in the quasi-elastic region. Examples of data[32] are shown in Fig. 16b. Calculations for some of these cases[34] are shown in Fig. 22. The characteristic V-shaped pattern is very nicely reproduced by the calculations. The qualitative explanation of this pattern is again rather simple. Fragments close in Z to the projectile and with substantial kinetic energy on the average have exchanged fewer nucleons than fragments farther removed in Z from the projectile. Thus less angular momentum is transferred to the former than to the latter fragments, giving rise to the rapid increase of the γ-ray multiplicity as one moves away from the projectile in either direction. This good agreement is consistent with the agreement observed between experiment and theory in Fig. 21 at the highest kinetic energies. From both of these figures one is tempted to conclude that particle exchange is sufficient to quantitatively explain the dependence of the angular momentum transfer upon kinetic energy loss, without invoking the excitation of giant collective modes. Apparently the same one-body theory that reproduces both the Z distributions and the angular distributions vs Z so satisfactorily, also handles the energy and angular momentum transfer more than adequately.

The final aspect to be considered is the Z dependence of the γ-ray multiplicity in the deep-inelastic region. Examples of data[32] are shown in Fig. 17 and of calculations[34] are given in Fig. 22. Again, the experimental data are reproduced quite well. It must be emphasized that in this energy region the calculation predicts near rigid rotation

throughout the Z range. Yet the rise of M_γ with decreasing Z, commonly considered a fingerprint of rigid rotation is conspicuously absent. The reason for this behavior is to be found in the angular momentum fractionation along the mass asymmetry coordinate as first inferred elsewhere. The main cause for angular momentum fractionation is the interaction time dependence upon ℓ. The high ℓ-waves are characterized by a short interaction time and cannot spread too far away from the entrance channel asymmetry. The low ℓ-waves are characterized by a longer interaction time and can populate asymmetries farther removed from the entrance channel. Consequently as one moves towards more extreme asymmetries, one selects progressively lower ℓ-waves.

Furthermore, at high angular momentum, the driving force is strongly directed towards the higher Z's and discourages any diffusion towards low Z's (see Fig. 23). As the angular momentum decreases, the driving force also diminishes and may even reverse its direction, thus allowing for a substantial diffusion to occur in the direction of the low Z's. Consequently the low Z's are selectively populated by low ℓ-waves and hence the lack of rise in the γ-ray multiplicity with increasing Z. An extreme case of angular momentum fractionation can be seen in Fig. 17c at the lowest Z's. Similar results have been obtained by other groups with similar approaches.[35]

e) <u>The Second Moments of the γ-Ray Multiplicities and Their Sources</u>

Recent measurements of the 2nd moments of the γ-ray multiplicities[36] indicate that they are substantially larger than the values expected from a $2\ell + 1$ distribution ($\sigma/\bar{I} = 0.35$). When the measurements are performed as a function of Z, the diffusion process which, as was

mentioned above, can fractionate the angular momentum, can also introduce a substantial second moment as can be seen from this simple exercise.

Let us use an analytic diffusion model without drift to interpret the dependence of the angular momentum distributions upon mass asymmetry.[37] The solution of the Fokker-Planck equation takes the form

$$P(Z,t) = [4\pi\mu_2 t]^{-1/2} \exp -(Z - Z_p)^2/2\mu_2 t$$

where P is the probability of producing a complex with asymmetry Z after an interaction time t, Z_p is the entrance channel asymmetry, and μ_2 is the spread coefficient. The cross section for a given impact parameter b can be expressed as:

$$\Phi(Z,b) = N[\tau(b)]^{-1/2}\, b \exp\left[-(Z - Z_p)^2/2\mu_2\, \tau(b)\right] \quad .$$

A simple form for the interaction time $\tau(b)$ is: $\tau(b) = \tau_0(1 - b/b_{max})$. By defining $\beta = (Z - Z_p)^2/2\mu_2\tau_0$, and by changing variables to $\eta = b/b_{max}$, one arrives at the distribution function

$$\Phi(\beta,\eta) = N[1 - \eta]^{-1/2}\ \beta^{-1/2}\, \eta \exp[-\beta/(1 - \eta)] \quad .$$

Given the angular momentum limits η_1, η_2 and the asymmetry β, one may write the moments of the angular momentum distribution as

$$\mu_m = \int_{\eta_1}^{\eta_2} \eta^m\, \Phi(\beta,\eta)d\eta = \int_{\eta_2}^{\eta_1} \frac{\eta^{m+1}}{[1 - \eta]^{1/2}} \exp -\beta/(1 - \eta)d\eta$$

By making the change of variable $x = (1 - \eta)^{-1}$ and defining $u_i = (1 - \eta_i)^{-1}$ for i = 1,2, one arrives at

$$\mu_m = \sum_{i=0}^{m+1} (-i)^i \binom{m+1}{i} \xi_i(u_1, u_2, \beta)$$

where

$$\xi_i(u_1, u_2, \beta) = \int_{u_1}^{u_2} x^{-(i+3/2)} e^{-\beta x} dx \quad .$$

The integrals ξ_i satisfy a recurrence relation

$$\xi_i = \frac{1}{i + 1/2} \left[\frac{e^{-u_1}}{u_1^{i+1/2}} - \frac{e^{-u_2}}{u_2^{i+1/2}} - \beta \xi_{i-1} \right] \quad .$$

In order to evaluate the desired integrals, it is sufficient to evaluate one of them separately. Application of the recurrence relation now allows evaluation of all desired ξ_i's, and thus all necessary μ_m's.

Consider a system in which essentially all impact parameters contribute to the deep inelastic process. In order to leave out events in which the kinetic energy in incompletely damped, it is assumed that $\eta_1 = 0$ and $\eta_2 = 0.9$, thus allowing 20% of the cross section for incompletely damped (QE) events. Three very striking features, shown in Fig. 24, emerge: (1) The mean angular momentum $\langle \eta \rangle$ decreases as a function of β. (2) The ratio $\rho = \sigma/\langle \eta \rangle$ exceeds the $2\ell + 1$ value for nearly all asymmetries. (3) The skewness γ changes sign as a function of asymmetry.

In order to compare with experiment, it is necessary to correlate β with Z. From previous work in fitting data from 620 Mev $^{86}Kr + {}^{197}Au$,

the following parameters are used: $\mu_2 = 6.6 \times 10^{21}\ e^2 sec^{-1}$, $\tau_0 = 4.0 \times 10^{-21}$ sec. To calculate the γ-ray multiplicity, $M_\gamma(Z)$, we assume rigid rotation. Then one has $M_\gamma(Z)/1/2\ell_{max} = f(Z)\langle \eta(\beta)\rangle$, where f(Z) is the fraction of the angular momentum tied up in the fragment spins. The curve of asterisks in Fig. 24 is a plot of this quantity. As can be seen, the multiplicities are approximately constant as a function of Z, in agreement with the data. Large values of γ are predicted in excess of those expected from a $2\ell + 1$ distribution.

Numerous sources of fragment angular momentum fluctuations can be found in the thermal excitation of angular momentum bearing normal modes, like bending, twisting, wriggling etc. Their effect will be considered in the next lecture. It sufficies here to say that, putting all the contributions together one can easily account for the experimental 2nd moments and still one may be left with some.

f) Alignment and Polarization of the Fragment Angular Momentum

The torques associated with the frictional forces acting between target and projectile during their interaction should induce a spin in the fragments aligned with the total angular momentum, and perpendicular to the reaction plane. Such an alignment can be effectively used to determine whether the fragments are scattered at positive or negative angles by determining, for instance, the circular polarization of the γ-rays emitted by the fragments. Clear-cut cases of positive scattering angles have been demonstrated for the strongly focussed reaction 612 MeV $^{86}Kr + ^{197}Au$ through the substantial negative circular polarization of the emitted γ-rays.[38]

Cases of weak polarization have been observed in the reaction Kr + Ag and have been interpreted in terms of contributions to the cross section from opposite sides of the interaction region.[38]

The circular polarization of γ-rays tests whether the fragment angular momentum points above or below the reaction plane and is therefore not very sensitive to angular momentum misalignment, provided that it is not so severe as to flip the very sign of the spin projection on the perpendicular to the reaction plane.

Spin misalignment can arise from the "thermal" excitation of normal modes in the intermediate complex that can bear angular momentum such as wriggling, tilting and bending modes.[39] This will be discussed in detail in the next lecture. One special way in which this can occur, is through the fluctuation in z projection of the transferred nucleons during the mass transfer.[35] In the case of the reaction Au + ^{620} MeV Kr, the thermal excitation of the collective modes generates approximately $17\hbar$ of random angular momentum to be coupled to about $27\hbar$ of aligned compontent of angular momentum arising from rigid rotation. This corresponds to an alignment parameter $P_{zz} \simeq 0.6$.

Attempts to measure the alignment have followed essentially two routes, namely the out-of-plane γ-ray anisotropy and the out-of-plane sequential fission fragment anisotropy.

A beautiful measurement of the out-of-plane anisotropy of resolved γ-ray lines in the reaction 96.5 MeV ^{16}O + ^{48}Ti indicates an alignment parameter ranging from $P_{zz} = 0.8$ to $P_{zz} = 0.5$ with increasing inelasticity of the reaction.[38]

The continuum γ-rays are more difficult to test because of the presence of a mixture of multipolarities. In the reaction Au + Xe, a window set on symmetric mass splitting allows one to observe fragments that are known from compound nuclear studies to deexcite at least 80% by stretched E2 decay. Preliminary studies of the out-of-plane angular distributions rule out deviations for isotropy larger than 30%. This is consistent with the alignment parameters $P_{zz} \cong 0.6$ if proper account is taken of the statistical γ-rays which are present with an abundance of ~ 20%.

The study of the out-of-plane angular distribution of sequential fission fragments is complicated by the fact that the fission fragments are not emitted exactly perpendicular to the angular momentum, but have r.m.s K projection $K_0 > 0$.

In the reaction Kr + Au at 620 MeV,[39] an out-of-plane r.m.s angular width of ~25° has been measured for the sequential fission fragments (see Fig. 25). Similar results have been reported for the reaction Kr + Bi[40] and U, Pb + ^{58}Ni, ^{90}Zr.[41] With the possible exclusion of U, all the systems give the same out-of-plane angular width of ~25°. For the reaction Au + Kr, one would calculate, assuming an equilibrium excitation of the collective modes, a random component of angular momentum leading to an average angular misalignment of ~32° - 33°. The presence of $K_0 > 0$ should increase the out-of-plane angular width even over such a value. The apparent inconsistency between the continuum γ-ray angular distribution and the out-of-plane sequential fission angular distribution and/or between the theory and the sequential fission data can be resolved in the following way. Sequential fission

does not occur with equal probability for all angular momenta. Quite to the contrary, it favors greatly the largest angular momenta. This will substantially reduce the effect of the random component R of the angular momentum, since

$$\theta \sim \sqrt{\frac{R^2}{I^2}}$$

and also reduces the effect of K_0 in a similar way. An indirect proof of this is available from the correlation between out-of-plane angle and fissionability in Pb + Ni,Zr.[41] When the fissionability is low, at small energy losses, the r.m.s angular width is $\sim 25°$. When the fissionability at large energy losses approaches unity, no great angular momentum discrimination can take place and the r.m.s angular width is close to 35°, in reasonable agreement with our theoretical expectations.

REFERENCES

1. For general reviews see, for instance: L.G.Moretto and R.Schmitt, J. de Phys. 37: C5 (1976) 109; W.U.Schröder and J.R.Huizenga, Ann. Rev. Nucl. Sci. 27 (1977) 465; M.Lefort and Ch.Ngô, Ann. Phys. 3 (1978) 5.

2. R.A.Broglia, C.M.Dasso, A.Winther, Phys. Lett. 53B (1974) 301; ibid 61B (1976) 113.

3. L.G.Moretto, J.S.Sventek and G.Mantzouranis, Phys. Rev. Lett. 42 (1979) 563.

4. See, for instance, D.H.E.Gross and H.Kalinowski, Phys. Lett. 48B (1974) 302.

5. L.G.Moretto and J.S.Sventek, Phys. Lett. 58B (1975) 26.

6. W.Nörenberg, Phys. Lett. 53B (1974) 289.

7. L.G.Moretto, B.Cauvin, P.Glässel, R.Jared, P.Russo, J.Sventek, and G.Wozniak, Phys. Rev. Lett. 36 (1976) 1069; P.Russo, R.P.Schmitt, G.J.Wozniak, R.C.Jared, P.Glässel, B.Cauvin, J.S.Sventek, and L.G.Moretto, Nucl. Phys. A281 (1977) 509.

8. R.P.Schmitt, G.Bizard, G.J.Wozniak and L.G.Moretto, Phys. Rev. Lett. 41 (1978) 1152.

9. J.Blocki, Y.Boneh, J.R.Nix, J.Randrup, M.Robel, A.J.Sierk, and W.J.Swiatecki, Ann. of Phys. 113 (1978) in press.

10. B.Cauvin, R.Jared, P.Russo, R.P.Schmitt, R.Babinet, and L.G.Moretto, Nucl. Phys. A301 (1977) 511.

11. B.Tamain, R.Chechik, H.Fuchs, F.Hanappe, M.Morjean, C.Ngô, J.Péter, M.Dakowski, B.Lucas, C.Mazur, M.Ribrag, and C.Signarbieux, Institut de Physique Nucleaire Orsay, Report IPNO-RC-79-02 (1979).

12. Y.Eyal, A.Gavron, I.Tserruya, Z.Fraenkel, Y.Eisen, S.Wald, R.Bass, C.R.Gould, G.Kreyling, R.Renfordt, K.Stelzer, R.Zitzmann, A.Gobbi, U.Lynen, H.Steltzer, I.Rude, R.Bock, Phys. Rev. Lett. 41 (1978) 625.

13. D.Hilscher, J.R.Birkelund, A.D.Hoover, W.U.Schröder, W.W.Wilcke, J.R.Huizenga, A.Mignerey, K.L.Wolf, H.F.Breuer, and V.E.Viola,Jr., Univ. of Rochester Nuclear Structure Research Laboratory Report UR-NSRL-189 (1979).

14. G.Wirth, W.Brüchle, H.Gäggeler, J.V.Kratz, M.Schädel, I.Warneke, G.Herrmann, M.Weis, R.Lucas, J.Poitou, Proceedings of the Internat'l Workshop on Gross Properties of Nuclei and Nuclear Excitations VII, Hirschegg, Austria, 1979, INKA-Conf-79-001-001/INKA-Conf-79-001-039, p.13.

15. B.Gatty, D.Guerreau, M.Lefort, X.Tarrago, J.Galin, B.Cauvin, J.Girard, and H.Nifenecker, Nucl. Phys. A253 (1975) 511.

16. M.Berlanger, A.Gobbi, F.Hanappe, U.Lynen, C.Ngô, A.Olmi, H.Sann, H.Stelzer, H.Richel, and M.F.Rivet, preprint.

17. G.Rudolf, A.Gobbi, H.Stelzer, U.Lynen, A.Olmi, H.Sann, R.G.Stokstad, and D.Pelte, preprint GSI-VP-12-78.

18. L.G.Moretto and J.S.Sventek, Proceedings of the Symposium on Macroscopic Features of Heavy Ion Collisions, Vol. 1, p.235 (1976) Argonne National Laboratory Report ANL/PHY-76-2.

19. W.Nörenberg, Z. Physik A274 (1975) 241; ibid A276 (1976) 84.

20. D.Agassi, C.M.Ko, H.A.Weidenmüller, Ann. Phys. 107 (1977) 140.

21. L.G.Moretto, J. Phys. Soc. Japan 44, Suppl. 7 (1978) 369.

22. J.Randrup, Nucl. Phys. A307 (1978) 319.

23. B.Cauvin, R.P.Schmitt, G.J.Wozniak, P.Glässel, P.Russo, R.C.Jared, J.B.Moulton and L.G.Moretto, Nucl. Phys. A294 (1978) 225.

24. J.R.Huizenga, J.R.Birkelund, W.U.Schröder, K.L.Wolf and V.E.Viola, Phys. Rev. Lett. 37 (1976) 885.

25. L.G.Moretto, J.Galin, R.Babinet, Z.Fraenkel, R.Schmitt, R.C.Jared, and S.G.Thompson, Nucl. Phys. A259 (1976) 172.

26. B.Heusch, C.Volant, H.Freiesleben, R.P.Chestnut, K.D.Hildebrand, F.Pühlhofer, W.F.W.Schneider, B.Kohlmeyer, and W.Pfeffer, Z. Physik A288 (1978) 391.

27. J.Galin, B.Gatty, D.Guerreau, M.Lefort, X.Tarrago, S.Agarwal, R.Babinet, B.Cauvin, J.Girard, and H.Nifenecker, Z. Physik A283 (1977) 173.

28. M.Beckerman and M.Blann, Phys. Rev. Lett. 38 (1977) 279.

29. G.J.Mathews and L.G.Moretto, Lawrence Berkeley Laboratory Report LBL-8972 (1979).

30. P.Glässel, R.S.Simon, R.M.Diamond, R.C.Jared, I.Y.Lee, L.G.Moretto, J.O.Newton, R.Schmitt and F.Stephens, Phys. Rev. Lett. 38 (1977) 331.

31. J.B.Natowitz, N.M.Namboodiri, P.Kasiraj, R.Eggers, L.Adler, P.Gontier, C.Cerutti and T.Alleman, Phys. Rev. Lett. 40 (1978) 751.

32. M.M.Aleonard, G.J.Wozniak, P.Glässel, M.M.Deleplanque, R.M.Diamond, L.G.Moretto, R.P.Schmitt, and F.S.Stephens, Phys. Rev. Lett. 40 (1978) 622.

33. J.S.Sventek and L.G.Moretto, Phys. Rev. Lett. 40 (1978) 697.

34. R.Regimbard, A.Behkami, G.J.Wozniak, R.P.Schmitt, J.S.Sventek, and L.G.Moretto, Phys. Rev. Lett. 41 (1978) 1355.

35. S.Ayik, G.Wolschin, and W.Nörenberg, Z. Physik A286 (1978) 271.

36. P.Christensen, F.Folkmann, O.Hansen, O.Nathan, N.Trautner, F.Videbaek, S.Y.van der Werf, H.C.Britt, R.P.Chestnut, H.Freiesleben, and F.Pühlhofer, Phys. Rev. Lett. 40 (1978) 1245.

37. J.S.Sventek, to be published.

38. W.Dünweber, J.de Boer, G.Graw, W.Hering, C.Lauterbach, H.Puchta, W.Trautman, U.Lynen, Proceedings of the Internat'l Workshop on Gross Properties of Nuclei and Nuclear Excitations VII A, INKA Conf-79-001-001-INKA-Conf-79-001-039 (1979), p.27, and references therein.

39. G.J.Wozniak, R.P.Schmitt, P.Glassel, R.C.Jared, G.Bizard, and L.G.Moretto, Phys. Rev. Lett. 40 (1978) 1436.

40. P.Dyer, R.J.Puigh, R.Vandenbosch, T.D.Thomas, and M.S.Zisman, Phys. Rev. Lett. 39 (1977) 392.

41. H.J.Specht, Lecture Notes in Physics 92 (1979) 1.

This work was done under the auspices of the Nuclear Physics Division of the U.S. Department of Energy.

FIGURE CAPTIONS

Fig. 1. Contour plots of the cross section in the total kinetic energy angle plane for various exit channel asymmetries in the reaction 620 MeV $^{86}Kr + ^{197}Au$.[7]

Fig. 2. a) Missing charge vs. total exit channel kinetic energy for various bombarding energies in the reaction $^{20}Ne + ^{63}Cu$.
b) Missing charge vs. excitation energy.[8]

Fig. 3. Masses prior to evaporation and number of evaporated neutrons vs. the atomic number of the fragment prior to evaporation. The solid circles and the open triangles refer to the heavy and light fragments respectively. For the significance of the lines, see text.[10]

Fig. 4. Ratio between the number of neutrons emitted by the two fragments vs. the mass ratio of the two fragments in the reaction 400 MeV Cu + Au.[11]

Fig. 5. Center of mass kinetic energy spectra of the neutrons associated with the two fragments in the same reaction as in Fig. 4.[11]

Fig. 6. Ratio of the mean number of neutrons emitted by the two fragments ν_1/ν_2 vs. the mean kinetic energy loss for the same reactions as in Fig. 4.[11]

Fig. 7. Variances of the distributions in Z at fixed mass asymmetry vs. excitation energy for deep inelastic fragments from the reaction 6.9 MeV/u $^{136}Xe + ^{197}Au$. The dashed curve indicates the expected variance from quantal fluctuations. The solid curve is the prediction for classical statistical fluctuations.[14]

Fig. 8. The quantal (curve 1) and classical (curve 2) widths of the Z distribution for fixed mass asymmetry vs. excitation energy. Curve 3 is the sum of both contributions and the triangle indicates the experimental value.[3]

Fig. 9. Widths of the Z distributions for several masses vs. the total kinetic energy for the reaction $^{86}Kr + ^{98}Mo$.[16]

Fig. 10. a) Contour plot of the cross section in the total kinetic energy-atomic number plane for the reaction $^{86}Kr + ^{166}Er$. The parallel lines between E_{Coul} and Q_{gg} are 20 MeV apart.[17]

b) Center of mass charge distributions for various kinetic energy bins at various lab angles in the reaction $^{197}Au + ^{86}Kr$. The energy bins start 50 MeV below the Coulomb barrier of two touching spheres and increase in steps of 25 parallel to the Coulomb barrier.[18]

Fig. 11. Center of mass angular distribuitons for various fragment Z's produced in the reaction 620 MeV $^{86}Kr + ^{197}Au$.[7]

Fig. 12. Z distributions calculated from the diffusion model[21] for the reactions ^{197}Au and ^{181}Ta + 620 MeV ^{86}Kr. The dots are the experimental data.[7,23]

Fig. 13. Angular distributions for individual fragments calculated from the diffusion model[21] for the same reactions as in Fig. 12.

Fig. 14. Deep inelastic and fusion-fission components in the reaction 170 MeV Ar + $^{107,109}Ag$. The solid line represents the data and the calculated cross section.[29]

Fig. 15. a) Gamma-ray multiplicities vs. atomic number for the reactions 175 MeV ^{20}Ne + Ag at 90°(lab)[30] and for the reaction 237 MeV ^{40}Ar + ^{89}Y. In the lower part of the figure the average gamma ray energies

for the latter reaction are also given.[31] b) Gamma-ray multiplicity vs. atomic number for the reaction $^{107,109}Ag$ + 288 MeV ^{40}Ar (curves) and $^{107,109}Ag$ + 340 MeV ^{40}Ar (open squares) [Author's unpublished data].

Fig. 16. a) Gamma ray multiplicity vs. TKE for the reaction 476 MeV ^{56}Fe + $^{107,109}Ag$, for different Z bins. b) Gamma-ray multiplicity vs. atomic number[32] for the quasi-elastic components of the reactions ^{165}Ho, ^{197}Au + 618 MeV ^{86}Kr.

Fig. 17. a) Gamma-ray multiplicites vs. Z for the deep inelastic component in 618 MeV ^{86}Kr + $^{107,109}Ag$, ^{165}Ho and ^{197}Au.[32] b) Same as in a) for the reaction 470 MeV ^{56}Fe + $^{107,109}Ag$ [Author's unpublished data]. Notice the angular dependence of M_γ. c) Same as in a) for the reaction 340 MeV ^{40}Ar + Tb [Author's unpublished data]. Notice the precipitous drop of M_γ at low Z's.

Fig. 18. a) Lines of constant angular momentum in the Z, TKE plane without angular momentum transfer. b) Same as in a) for a rigidly rotating system. c) Qualitative expectations for the correct lines of existant angular momentum.

Fig. 19. a) Lines of constant angular momentum in the TKE vs. Z plane. b) An expanded view of a) including contours of constant cross section.

Fig. 20. The ratio of the charge widths calculated for energy cuts along the lines of constant angular momentum and of constant total kinetic energy vs. the bin number for the energy loss.

Fig. 21. Gamma ray multiplicity vs. total kinetic energy for three Kr induced reactions. The solid and dashed curves are fits to the data.[34]

Fig. 22. Gamma ray multiplicity vs. atomic number for three reactions. The open circles represent the quasi-elastic components and the solid circles the deep inelastic components. Solid curves are fits to the data.[34]

Fig. 23. Potential energies vs. the atomic number of one fragment for various angular momenta for the system in $^{86}Kr + ^{197}Au$.

Fig. 24. Mean angular momentum $\langle \eta \rangle$, its second moment σ, the relative function $\rho = \sigma/\langle \eta \rangle$ and the skewness γ vs. the asymmetry parameter β (see text) The asterisks represent the expected dependence of the gamma ray multiplicity upon β.[37]

Fig. 25. FWHM of the out of plane fission and non-fission components as a function of Z.

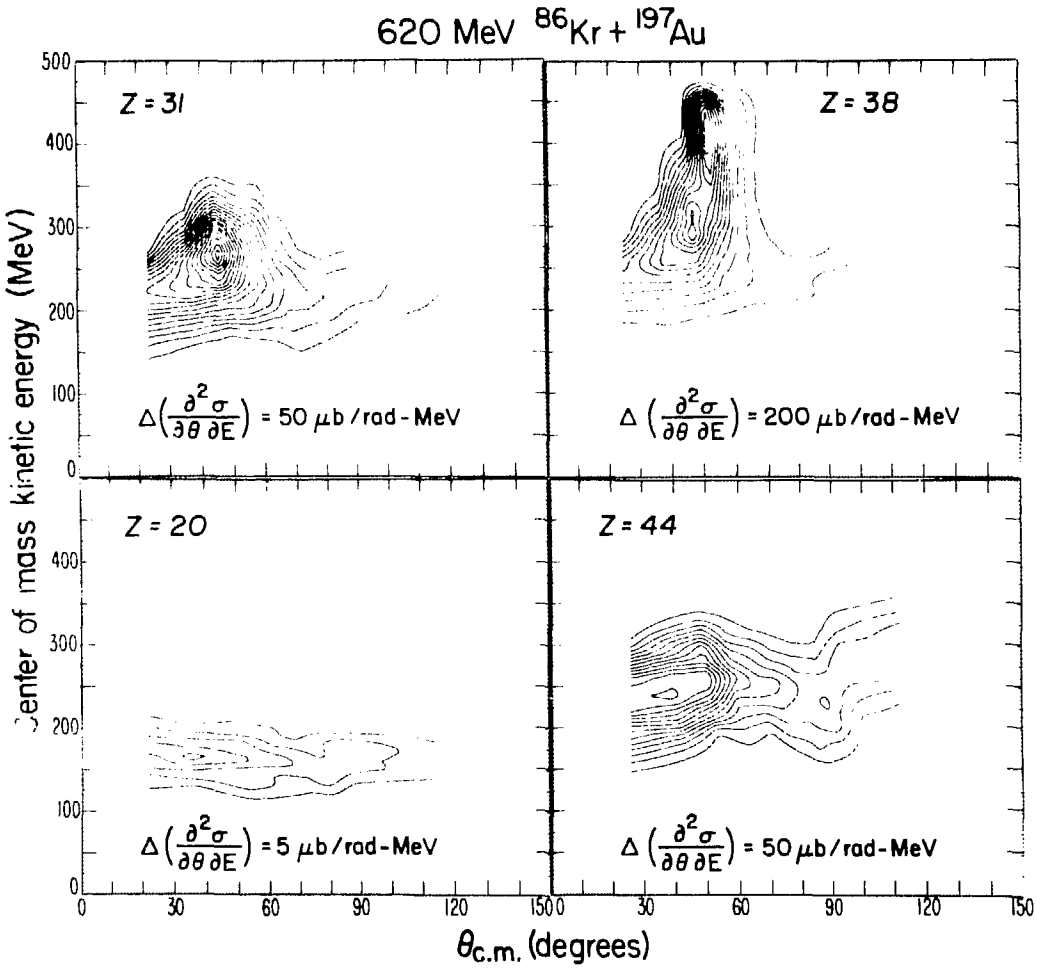
620 MeV ^{86}Kr + ^{197}Au
Z = 31
Z = 38
Z = 20
Z = 44
$\Delta\left(\frac{\partial^2\sigma}{\partial\theta\,\partial E}\right)$ = 50 μb/rad-MeV
$\Delta\left(\frac{\partial^2\sigma}{\partial\theta\,\partial E}\right)$ = 200 μb/rad-MeV
$\Delta\left(\frac{\partial^2\sigma}{\partial\theta\,\partial E}\right)$ = 5 μb/rad-MeV
$\Delta\left(\frac{\partial^2\sigma}{\partial\theta\,\partial E}\right)$ = 50 μb/rad-MeV
Center of mass kinetic energy (MeV)
$\theta_{c.m.}$ (degrees)
0
100
200
300
400
500
30
60
90
120
150
XBL 761-2089

Fig. 1

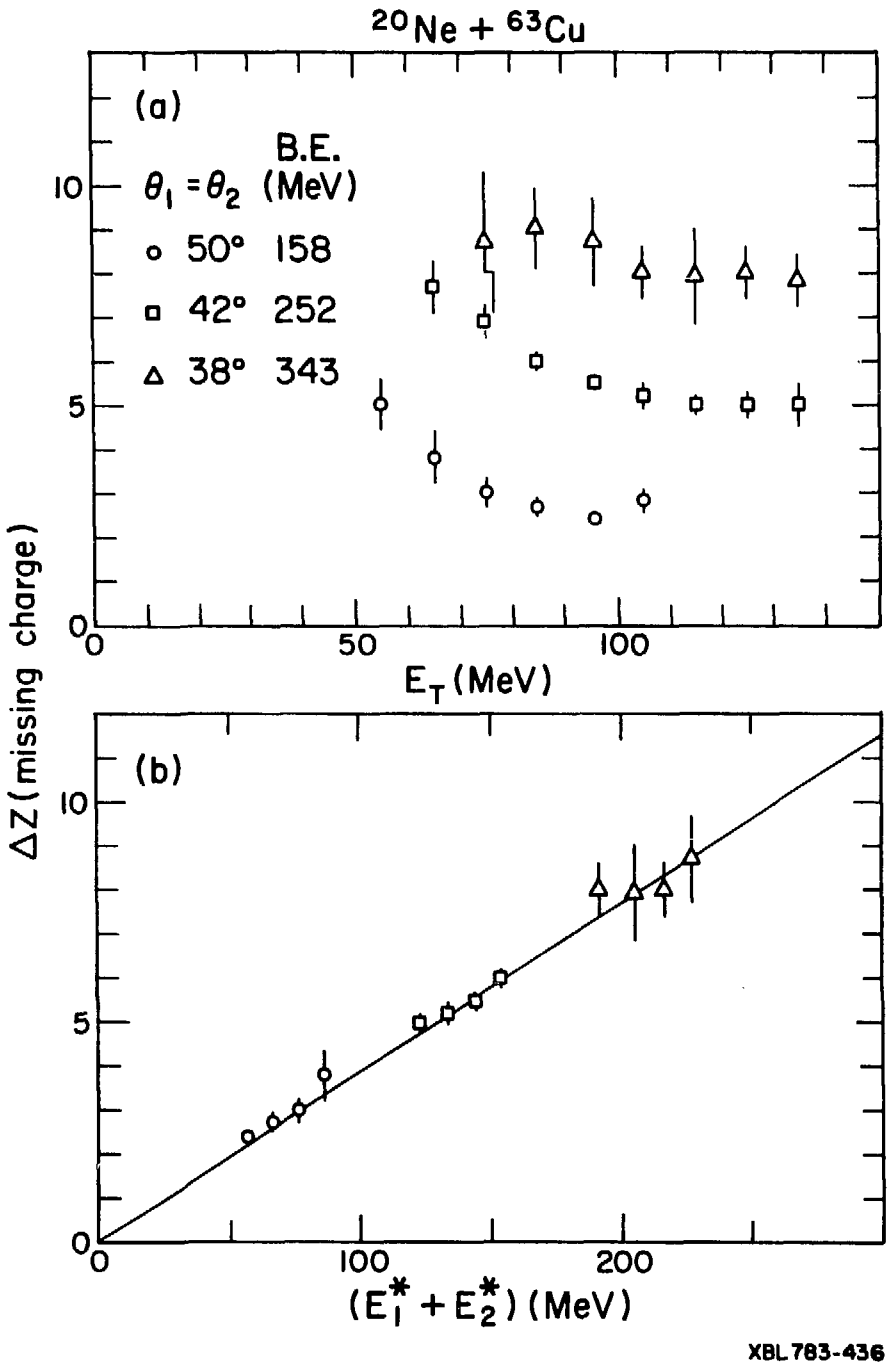
$^{20}Ne + ^{63}Cu$
(a)
B.E.
$\theta_1 = \theta_2$ (MeV)
50° 158
42° 252
38° 343
E_T (MeV)
ΔZ (missing charge)
(b)
$(E_1^* + E_2^*)$ (MeV)
XBL 783-436

Fig. 2.

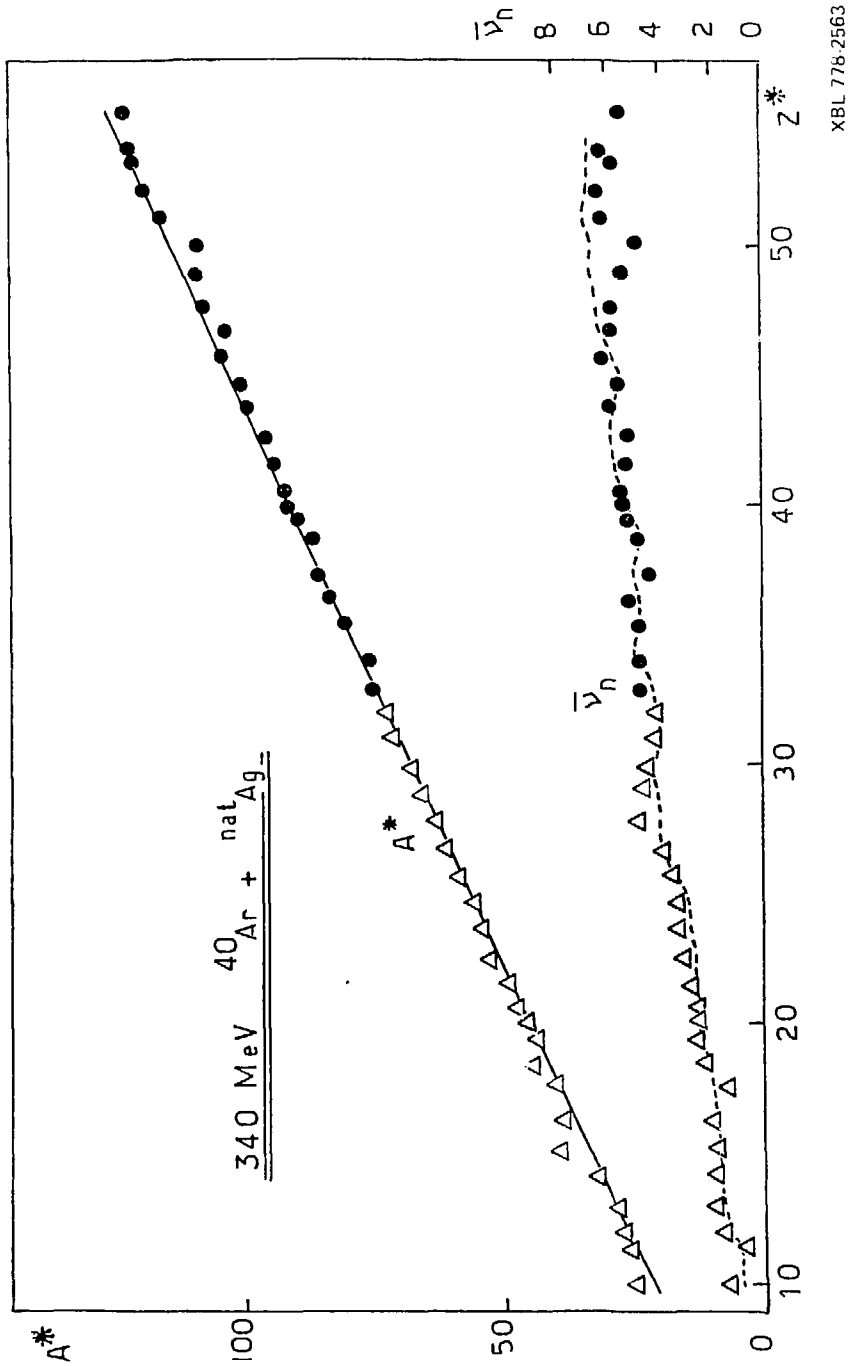

Fig. 3

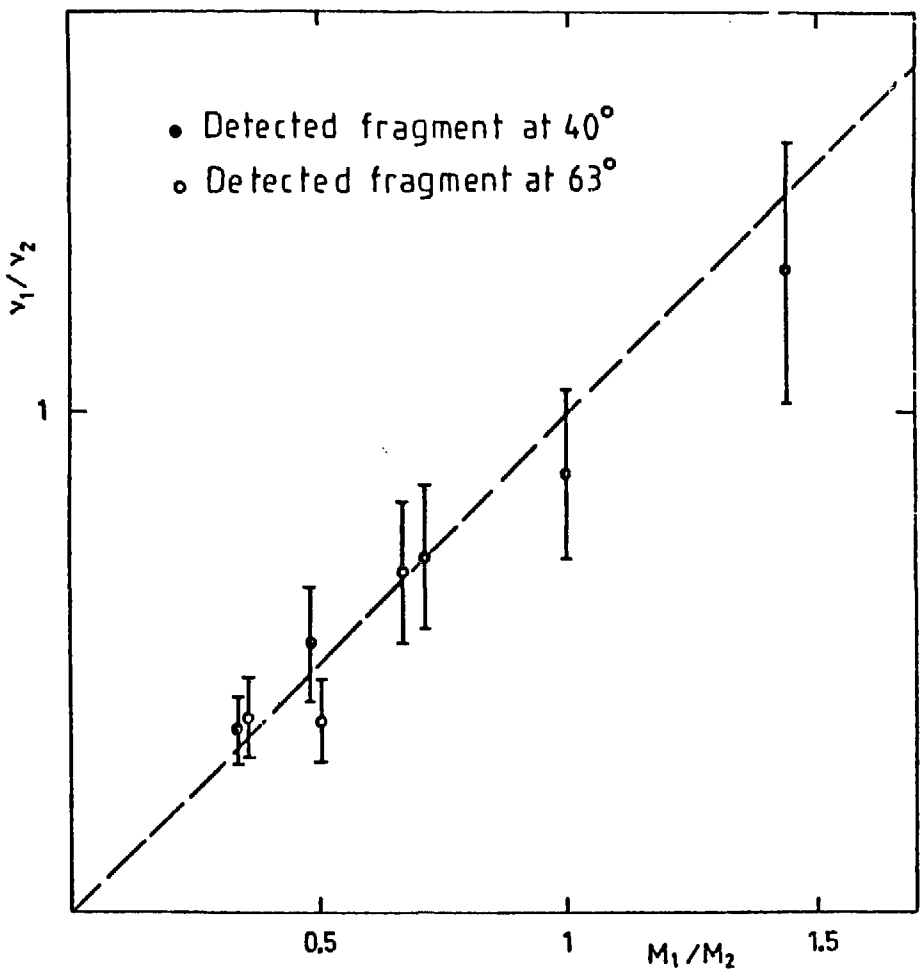
• Detected fragment at 40°
∘ Detected fragment at 63°
ν_1/ν_2
1
0.5
1
1.5
M_1/M_2

Fig. 4.

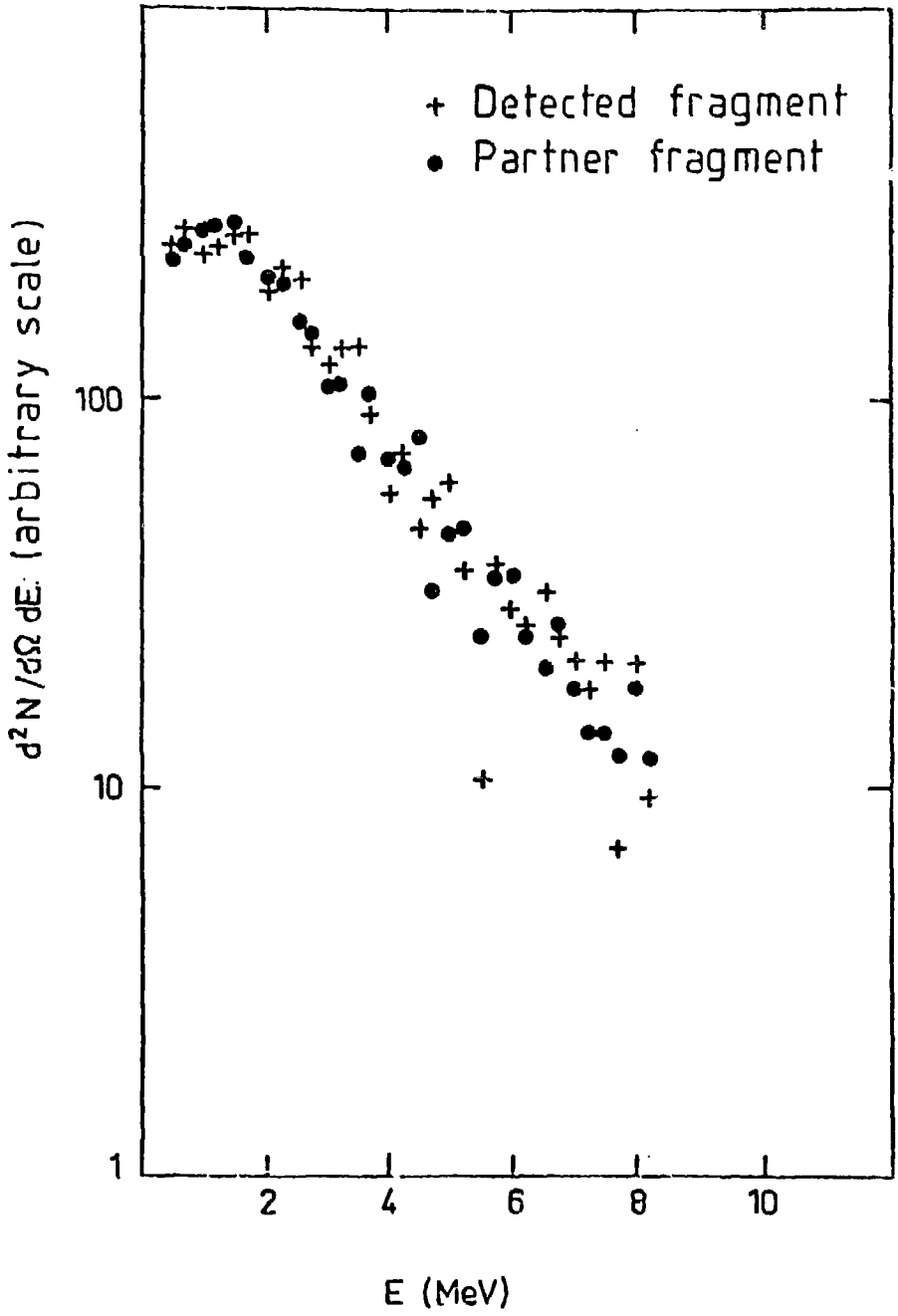
+ Detected fragment
● Partner fragment
$d^2N/d\Omega\, dE$ (arbitrary scale)
100
10
1
2
4
6
8
10
E (MeV)

Fig. 5

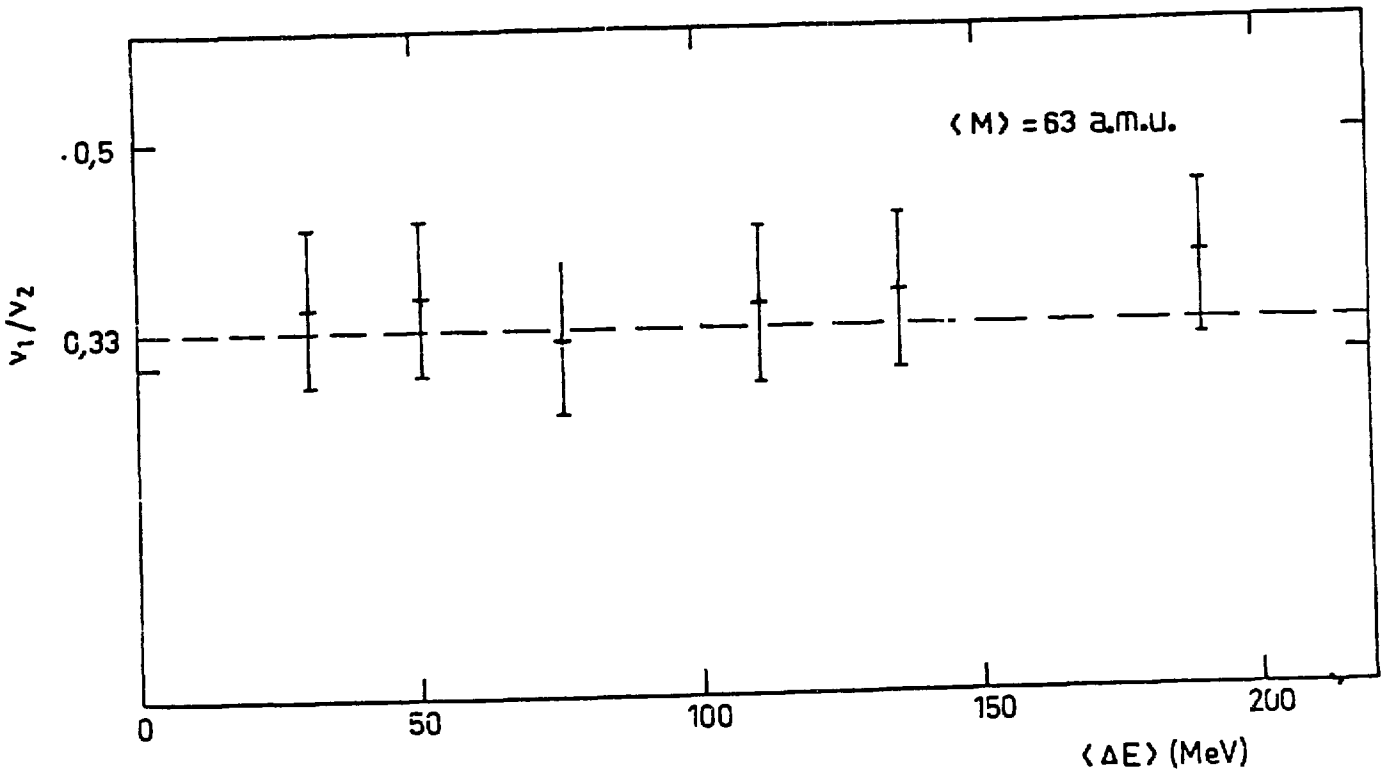

Fig. 6

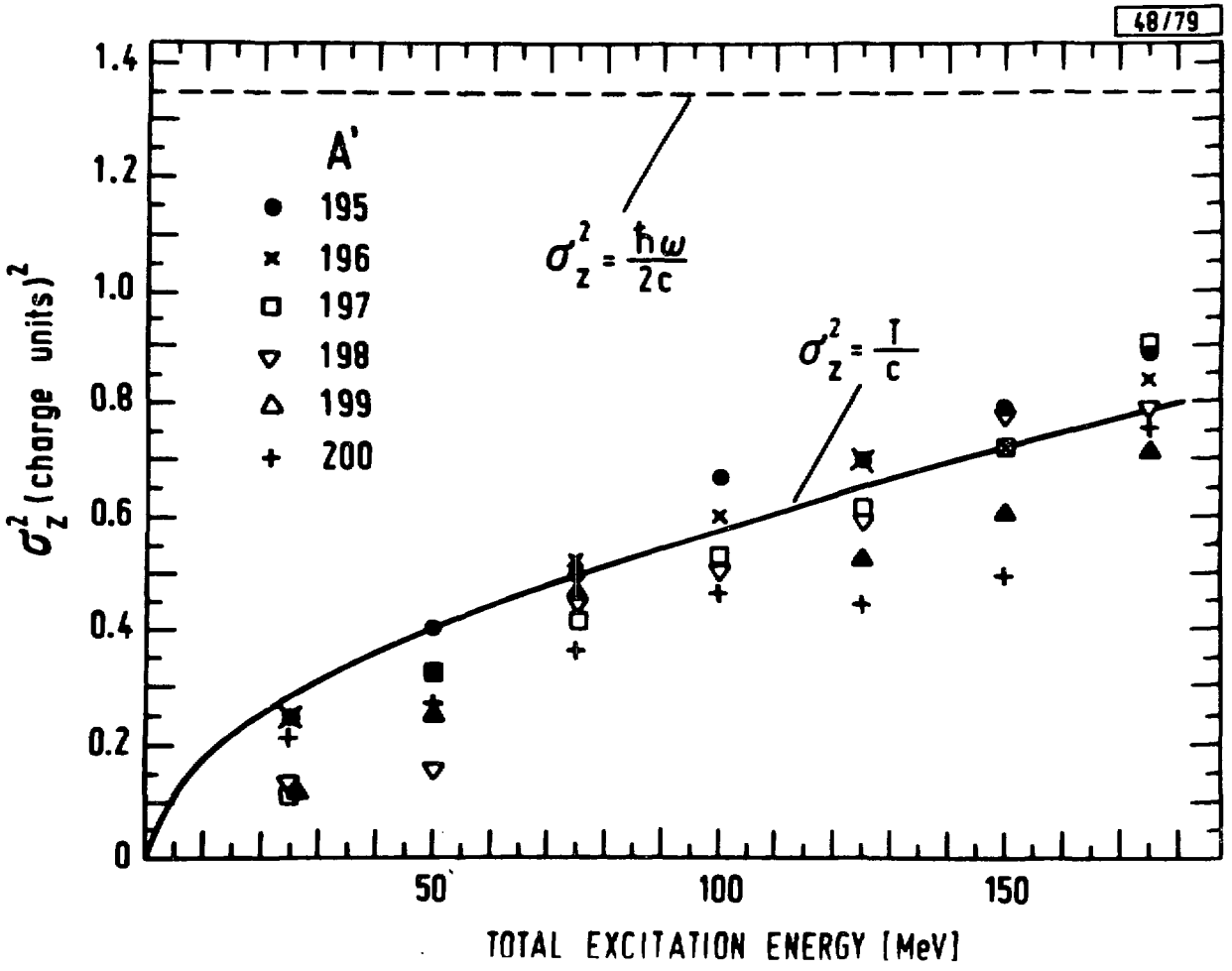

XBL 795-9813

Fig. 7

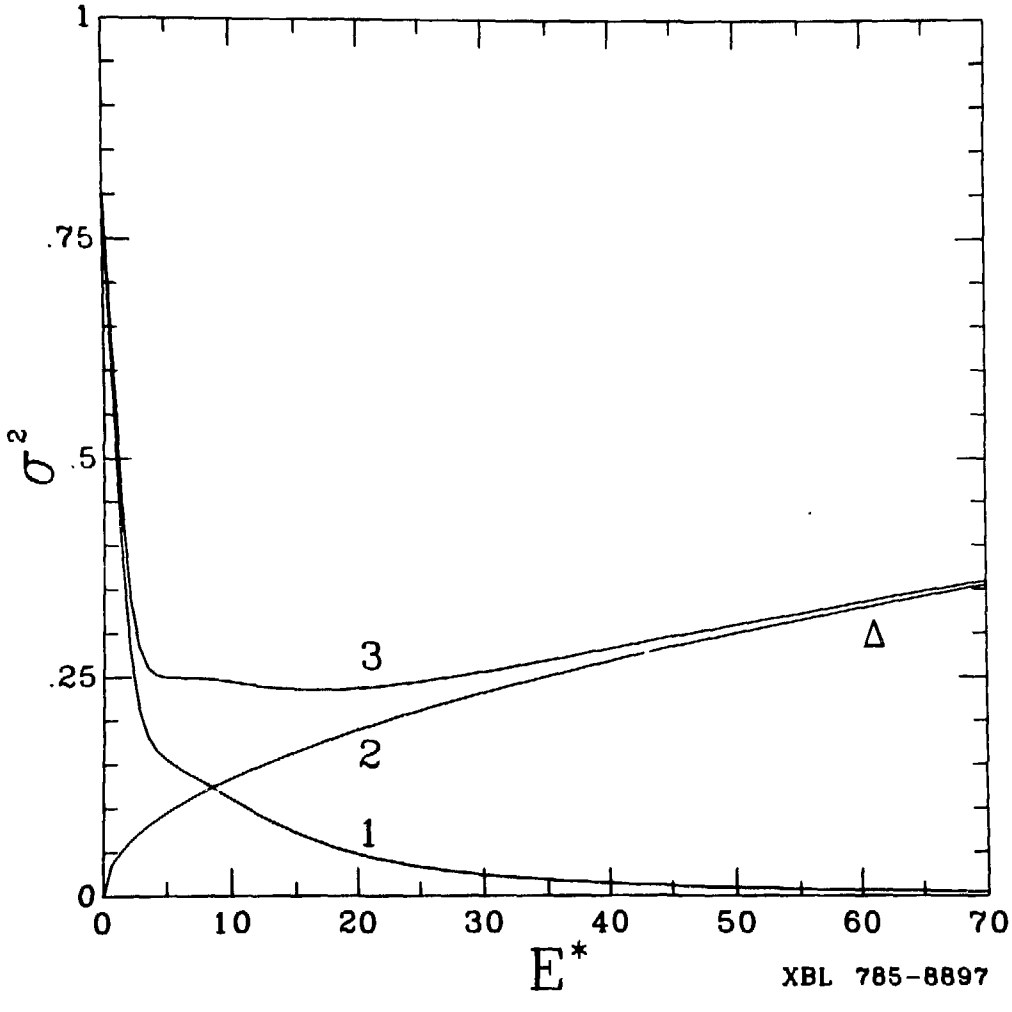

Fig. 8

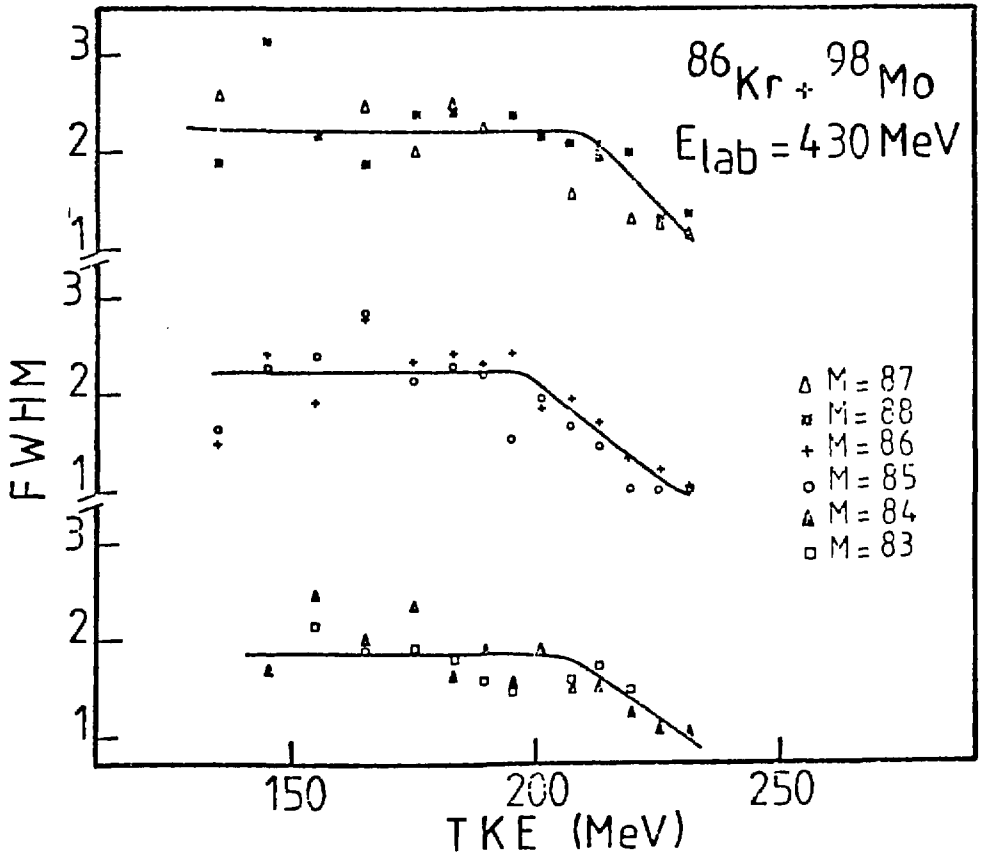
$^{86}Kr + ^{98}Mo$
$E_{lab} = 430$ MeV
FWHM
TKE (MeV)
150
200
250
1
2
3
Δ M = 87
M = 88
+ M = 86
o M = 85
▲ M = 84
□ M = 83

Fig. 9

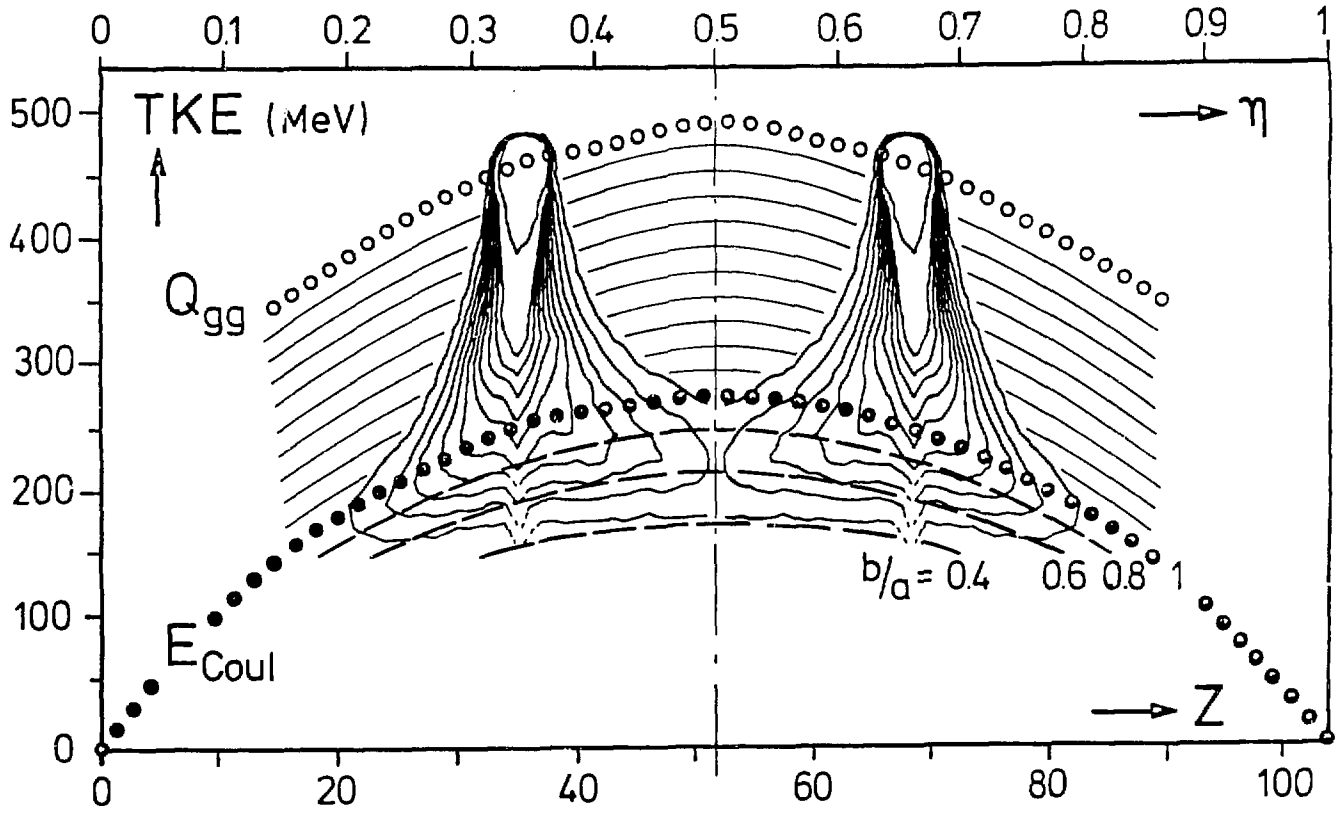
0
0.1
0.2
0.3
0.4
0.5
0.6
0.7
0.8
0.9
1
500
400
300
200
100
0
TKE (MeV)
η
Q_{gg}
E_{Coul}
b/a = 0.4
0.6
0.8
1
Z
0
20
40
60
80
100

Fig. 10a

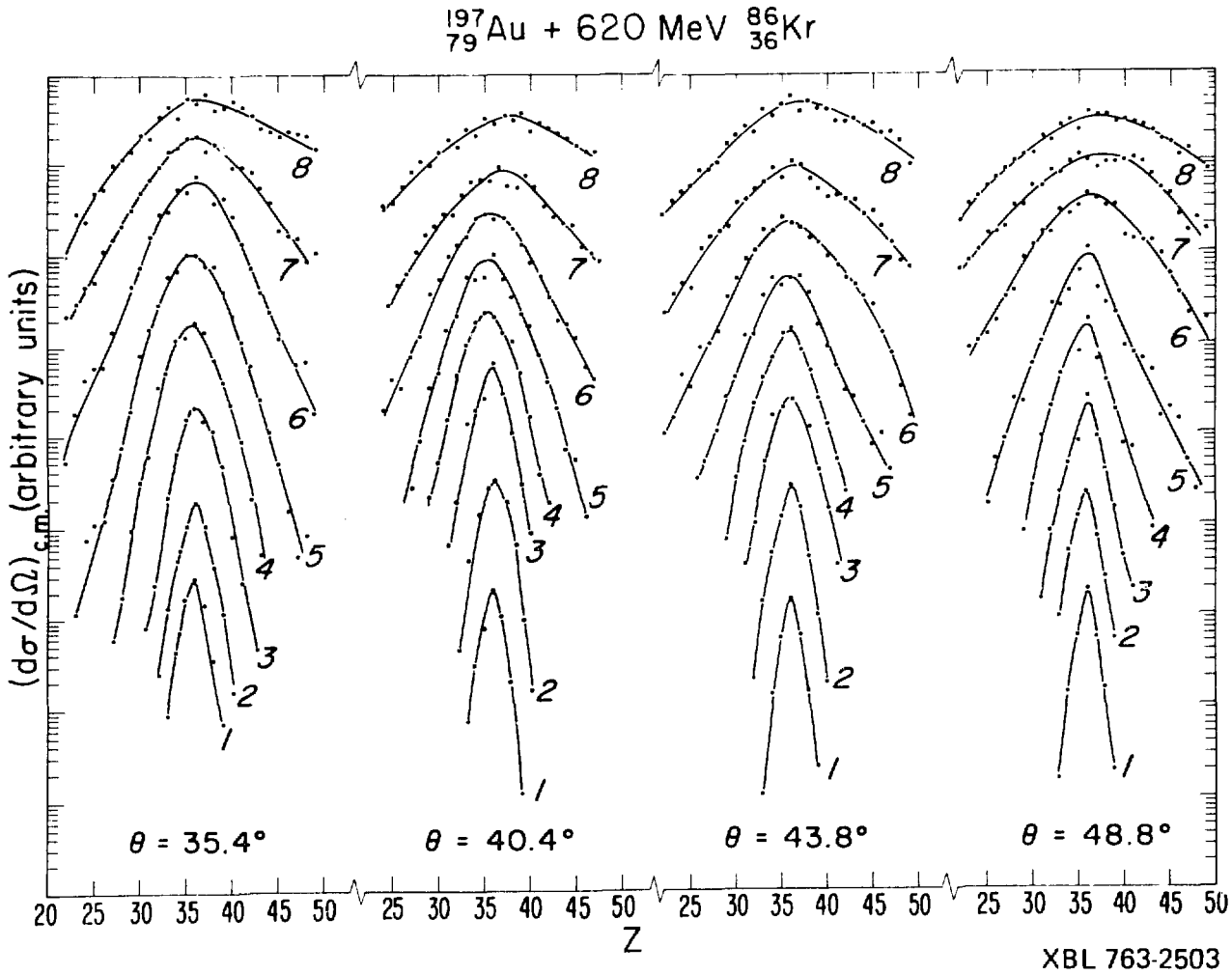
$^{197}_{79}$Au + 620 MeV $^{86}_{36}$Kr
$(d\sigma/d\Omega)_{c.m.}$ (arbitrary units)
θ = 35.4°
θ = 40.4°
θ = 43.8°
θ = 48.8°
20 25 30 35 40 45 50 25 30 35 40 45 50 25 30 35 40 45 50 25 30 35 40 45 50
Z
XBL 763-2503

Fig. 10b

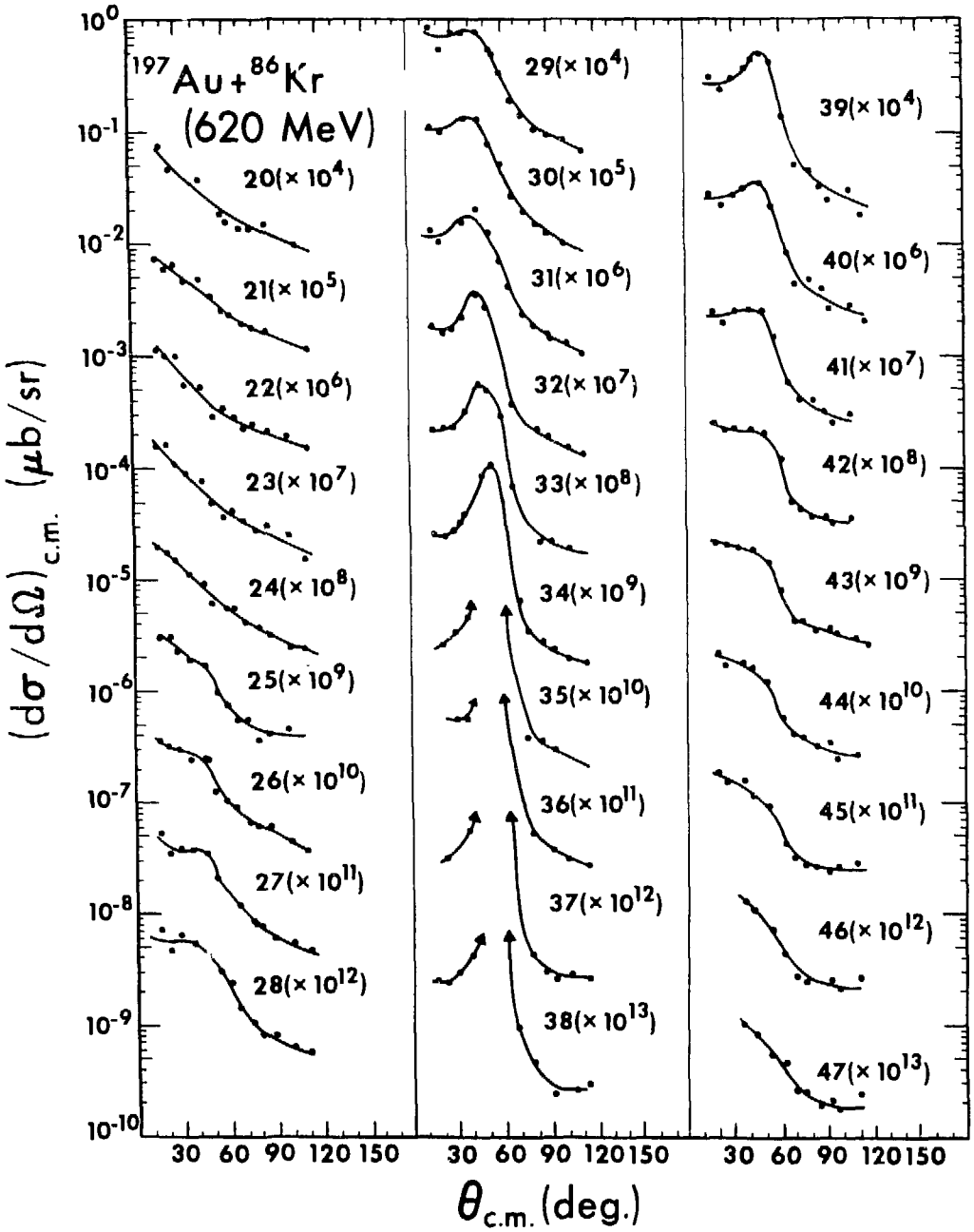
^{197}Au+^{86}Kr
(620 MeV)
20(× 10^4)
21(× 10^5)
22(× 10^6)
23(× 10^7)
24(× 10^8)
25(× 10^9)
26(× 10^{10})
27(× 10^{11})
28(× 10^{12})
29(× 10^4)
30(× 10^5)
31(× 10^6)
32(× 10^7)
33(× 10^8)
34(× 10^9)
35(× 10^{10})
36(× 10^{11})
37(× 10^{12})
38(× 10^{13})
39(× 10^4)
40(× 10^6)
41(× 10^7)
42(× 10^8)
43(× 10^9)
44(× 10^{10})
45(× 10^{11})
46(× 10^{12})
47(× 10^{13})
$(d\sigma/d\Omega)_{c.m.}$ (μb/sr)
$\theta_{c.m.}$ (deg.)
XBL 7512-9891

Fig. 11

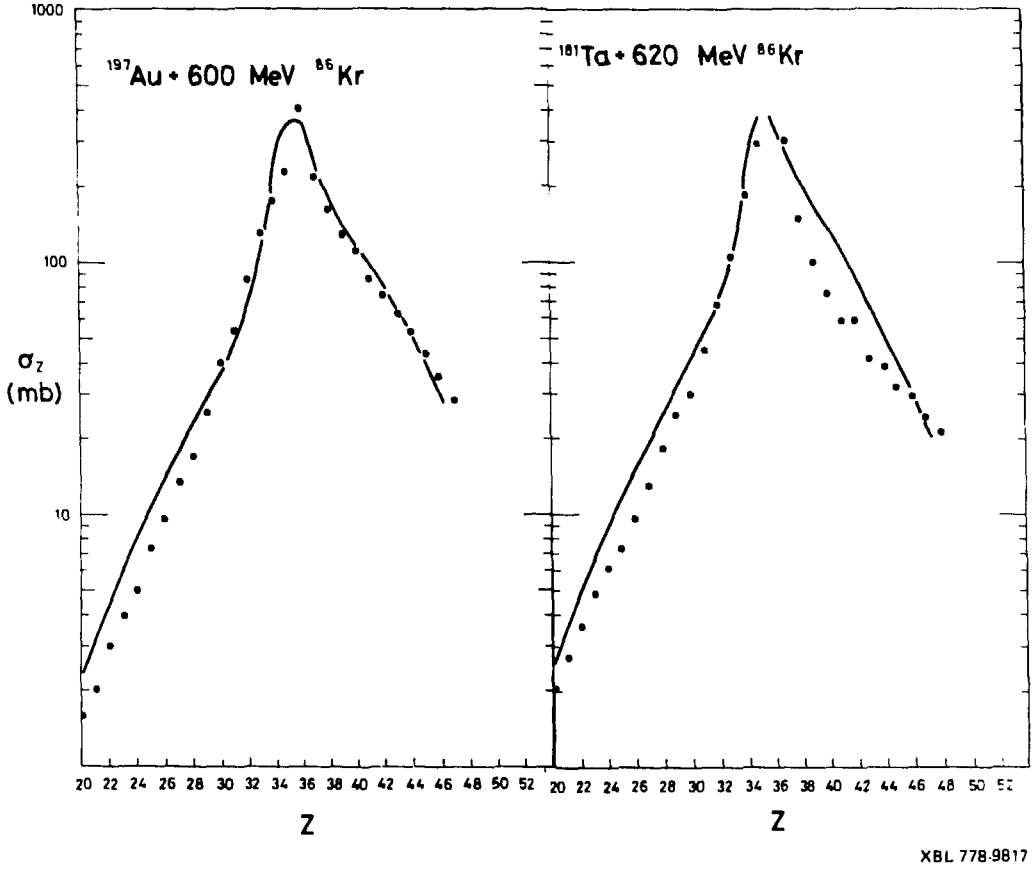
1000
100
10
σ_Z
(mb)
^{197}Au + 600 MeV ^{86}Kr
^{181}Ta + 620 MeV ^{86}Kr
20 22 24 26 28 30 32 34 36 38 40 42 44 46 48 50 52
Z
XBL 778-9817

Fig. 12

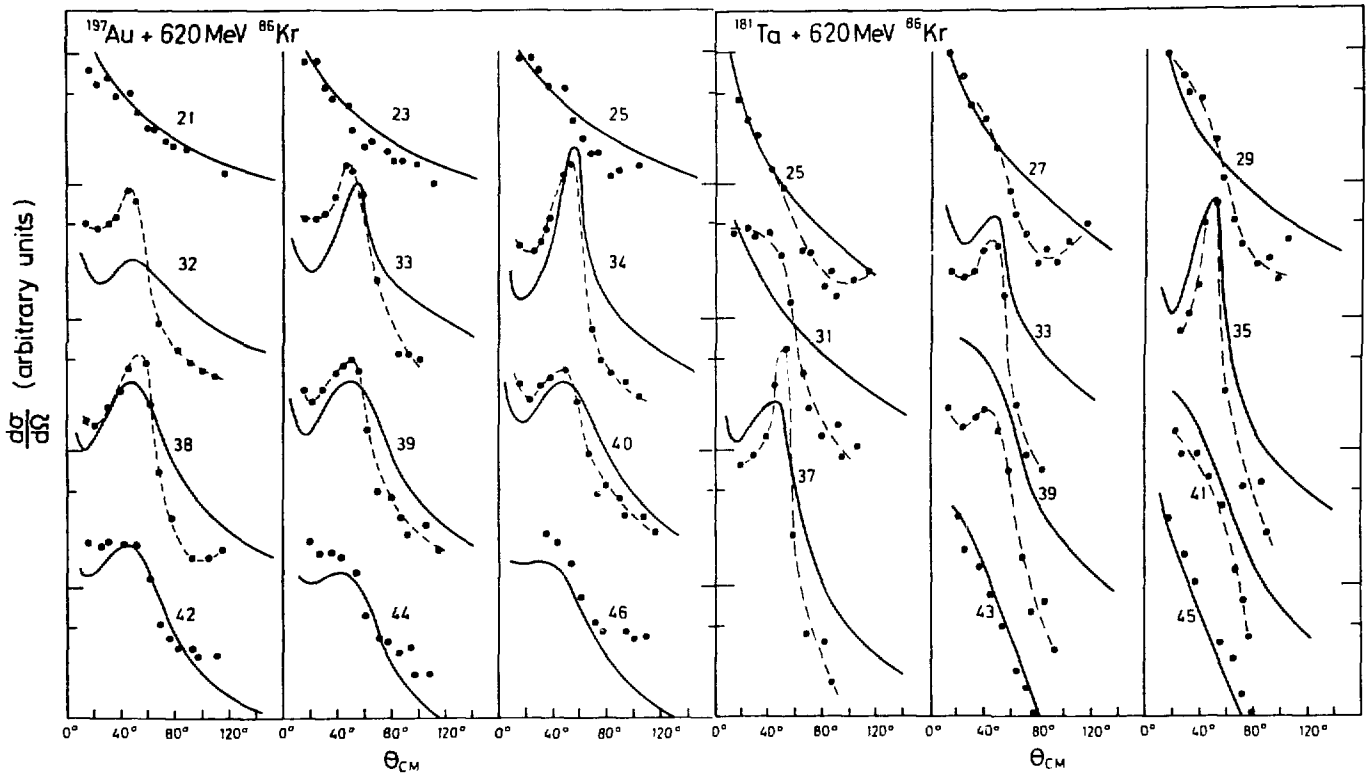

XBL 778-9908

Fig. 13

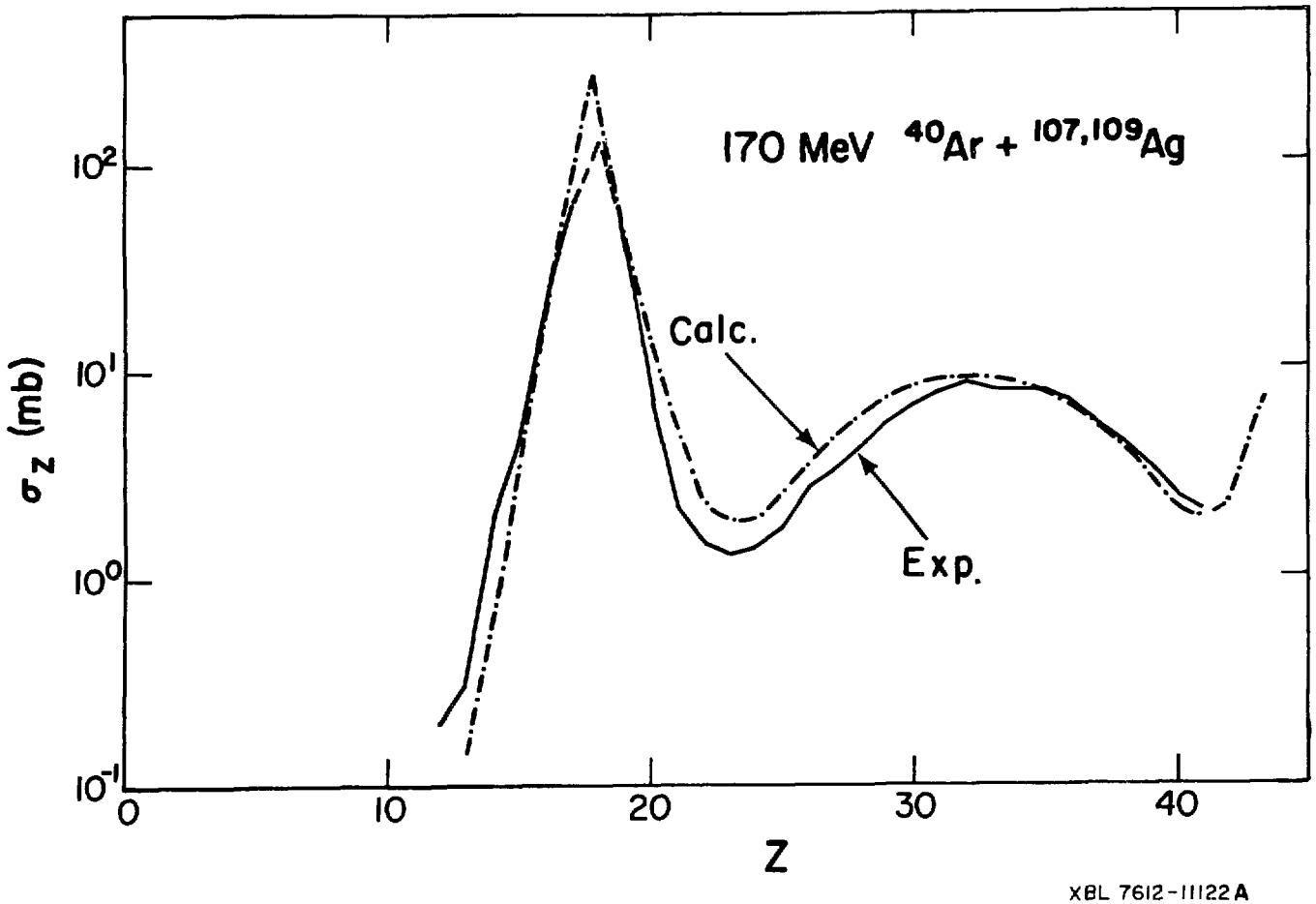
170 MeV ^{40}Ar + ^{107,109}Ag
Calc.
Exp.
σ_Z (mb)
10^2
10^1
10^0
10^{-1}
0
10
20
30
40
Z
XBL 7612-11122A

Fig. 14

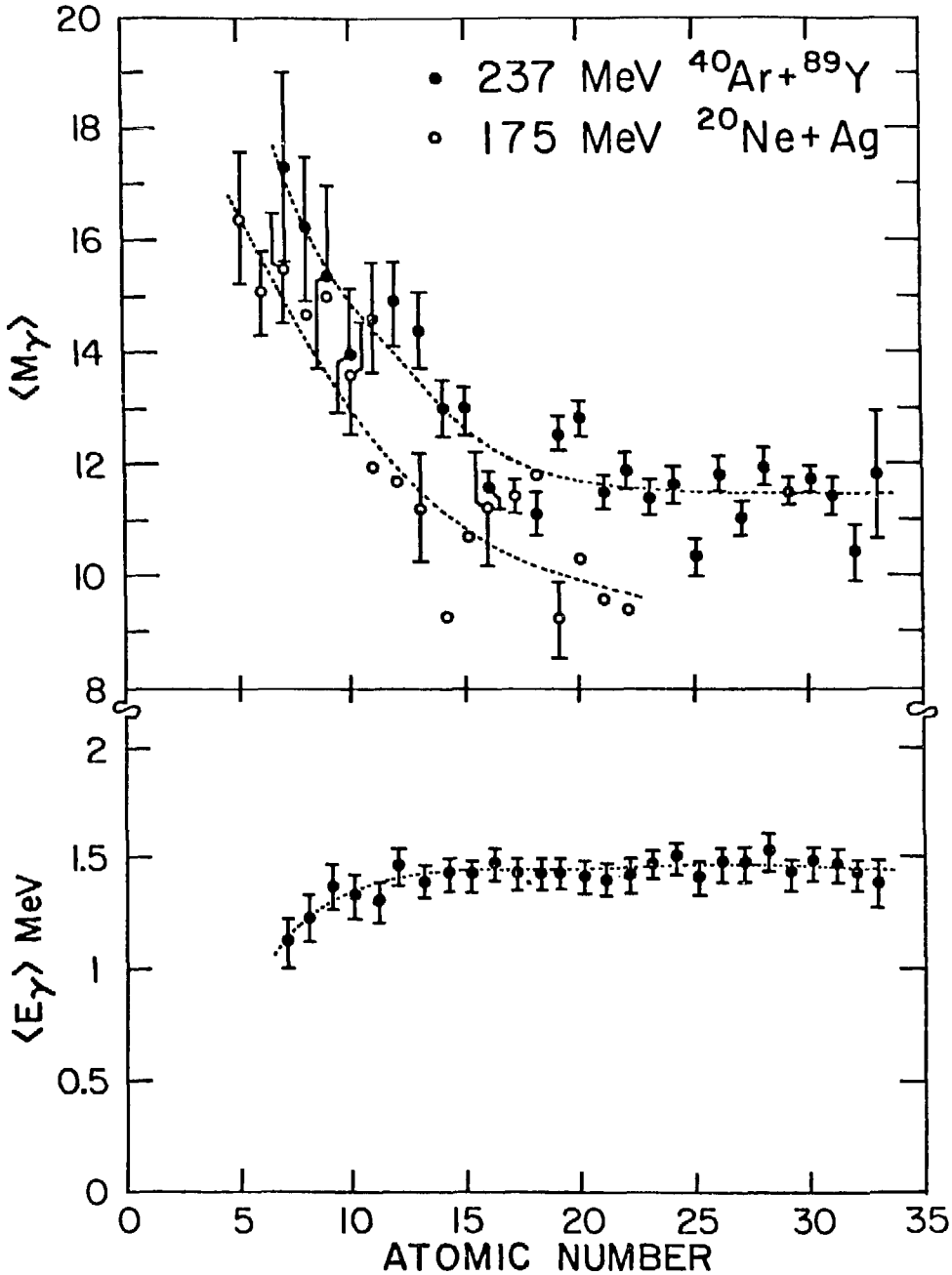
237 MeV ^{40}Ar+^{89}Y
175 MeV ^{20}Ne+Ag
⟨M$_\gamma$⟩
⟨E$_\gamma$⟩ MeV
ATOMIC NUMBER
20
18
16
14
12
10
8
2
1.5
1
0.5
0
0
5
10
15
20
25
30
35

Fig. 15a

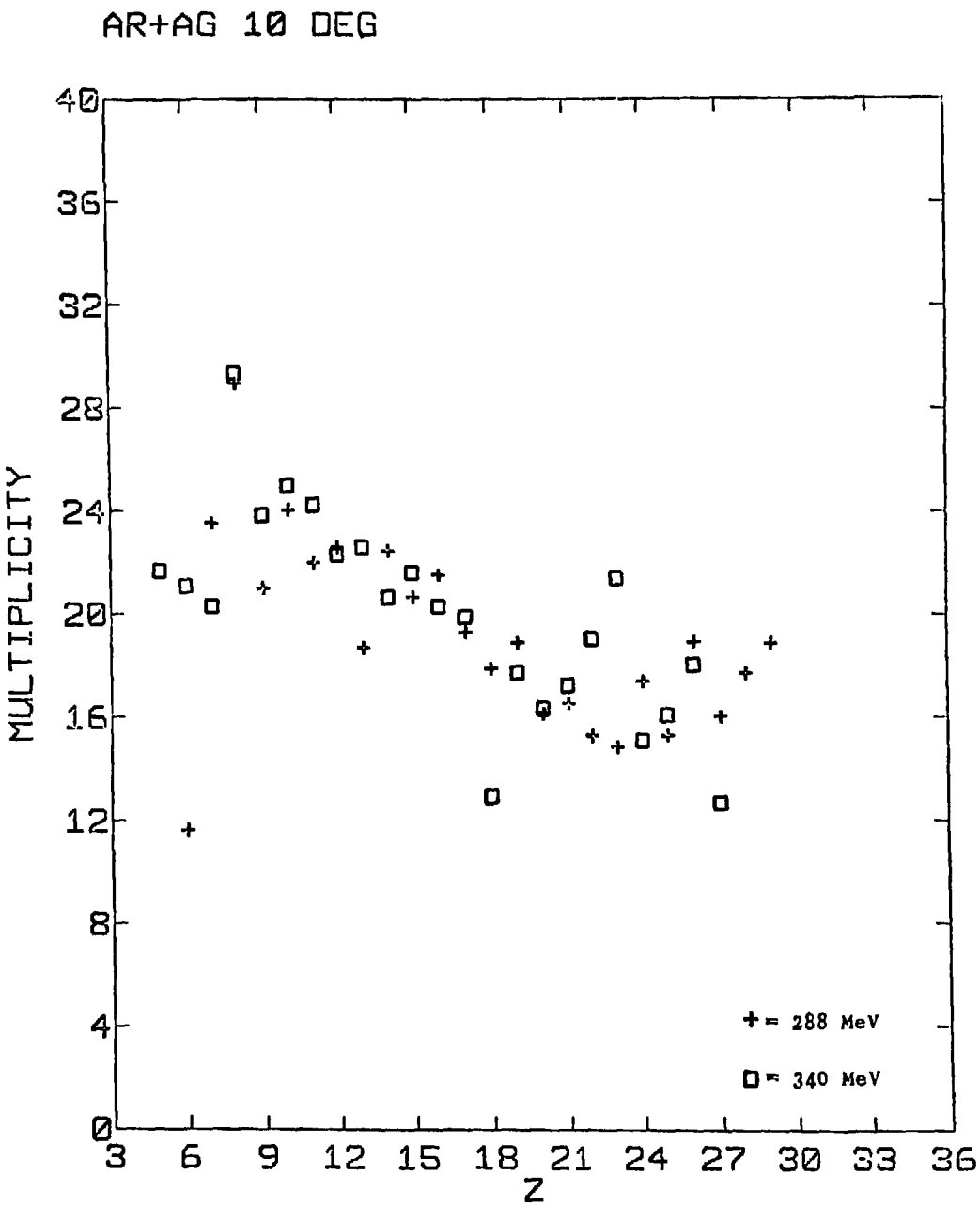

ADL 795-9881

Fig. 15b

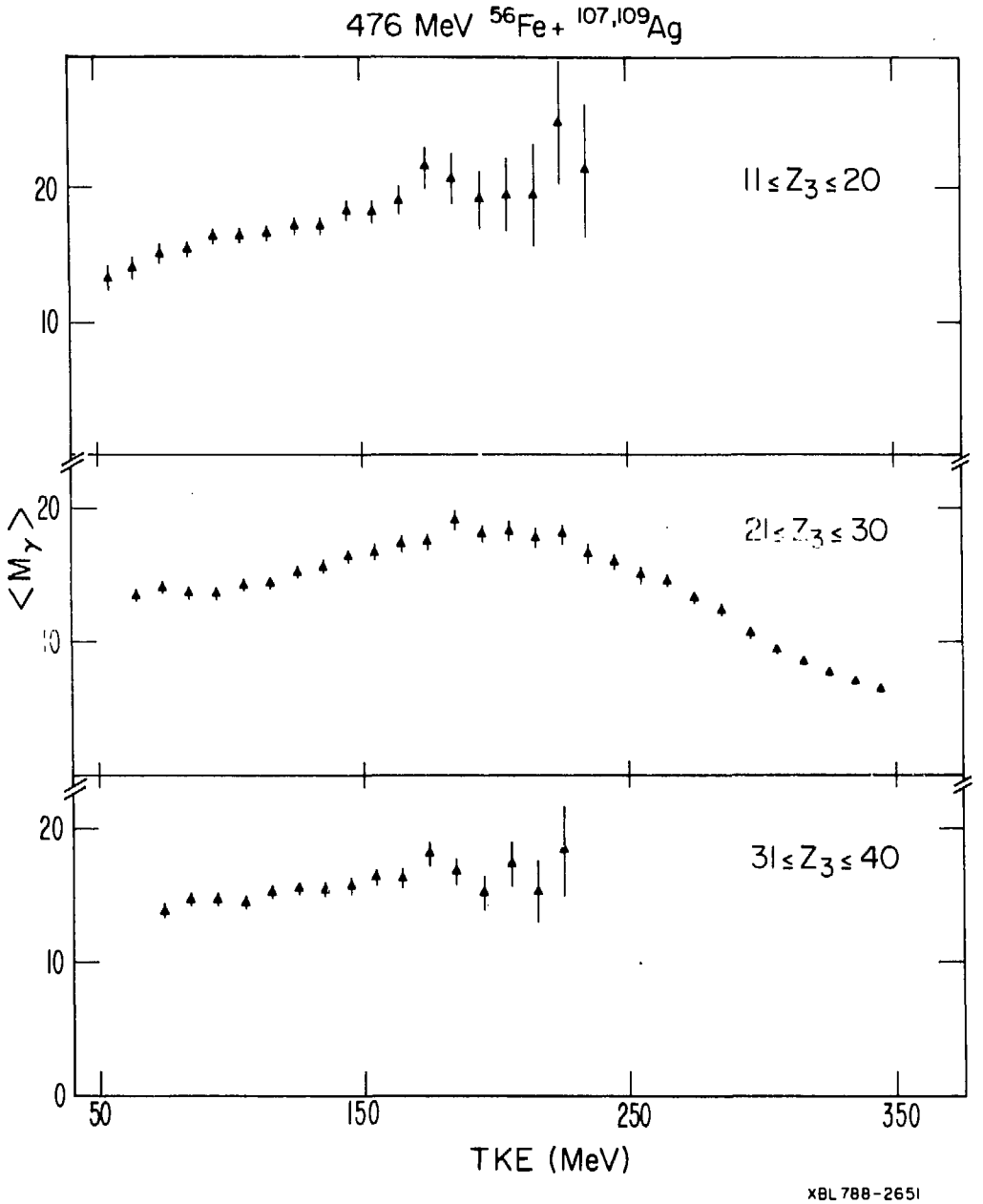
476 MeV $^{56}Fe + ^{107,109}Ag$
$11 \le Z_3 \le 20$
$21 \le Z_3 \le 30$
$31 \le Z_3 \le 40$
$\langle M_\gamma \rangle$
20
10
0
50
150
250
350
TKE (MeV)
XBL 788-2651

Fig. 16a

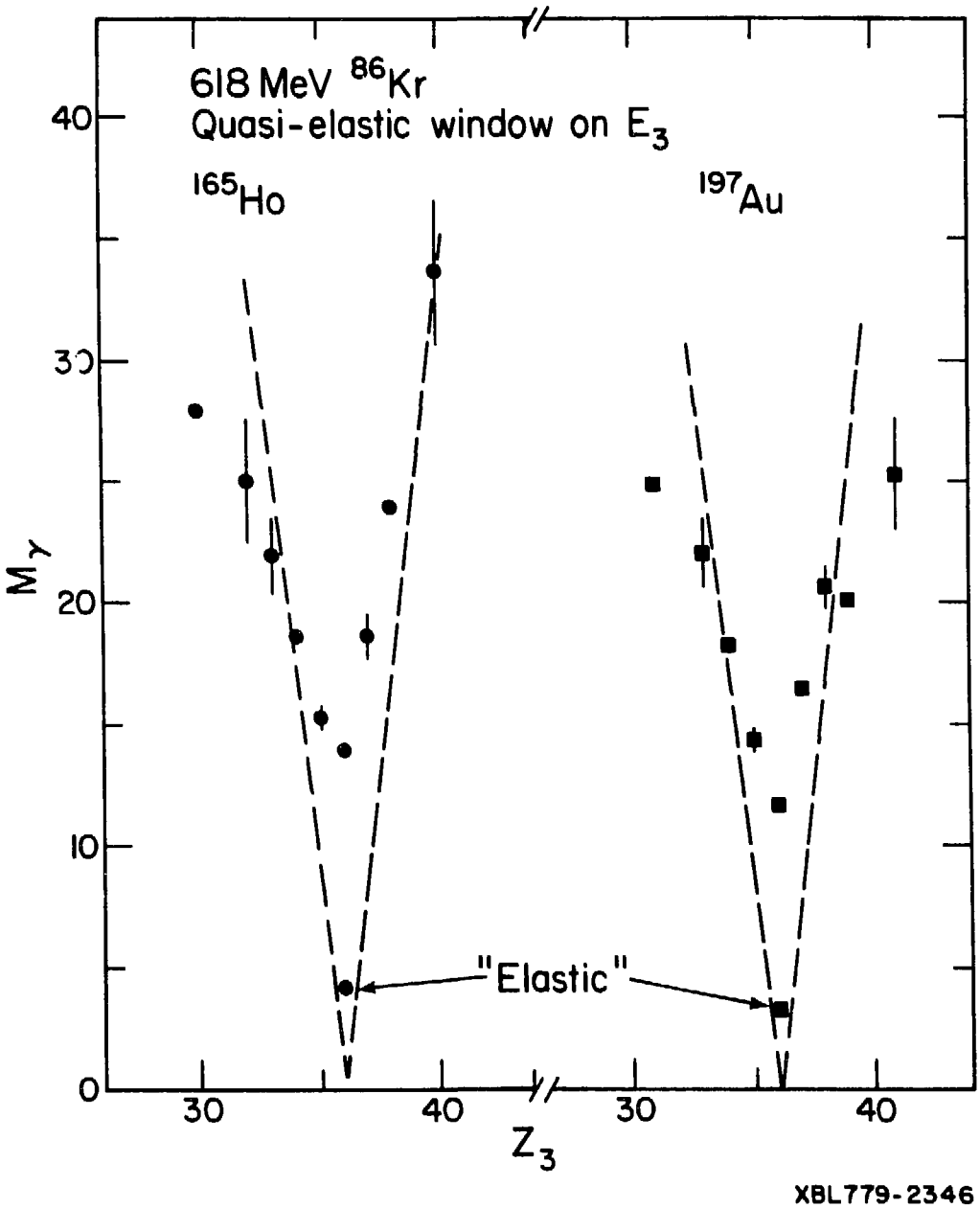
618 MeV ^{86}Kr
Quasi-elastic window on E_3
^{165}Ho
^{197}Au
"Elastic"
M_γ
Z_3
0
10
20
30
40
30
40
30
40
XBL779-2346

Fig. 16b

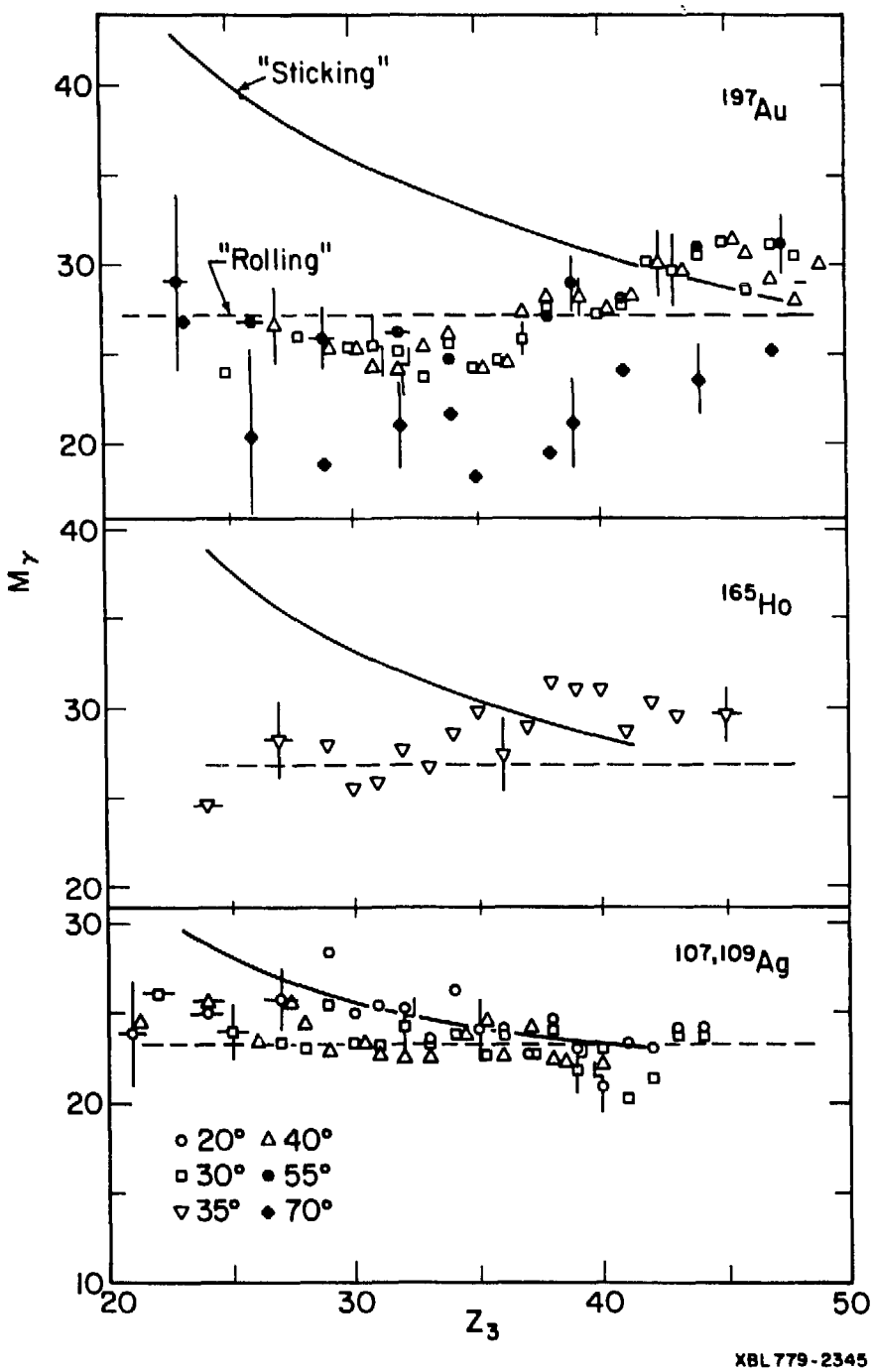
"Sticking"
"Rolling"
197Au
165Ho
107,109Ag
M_γ
Z_3
40
30
20
10
20
30
40
50
○ 20° △ 40°
□ 30° ● 55°
▽ 35° ◆ 70°
XBL 779-2345

Fig. 17a

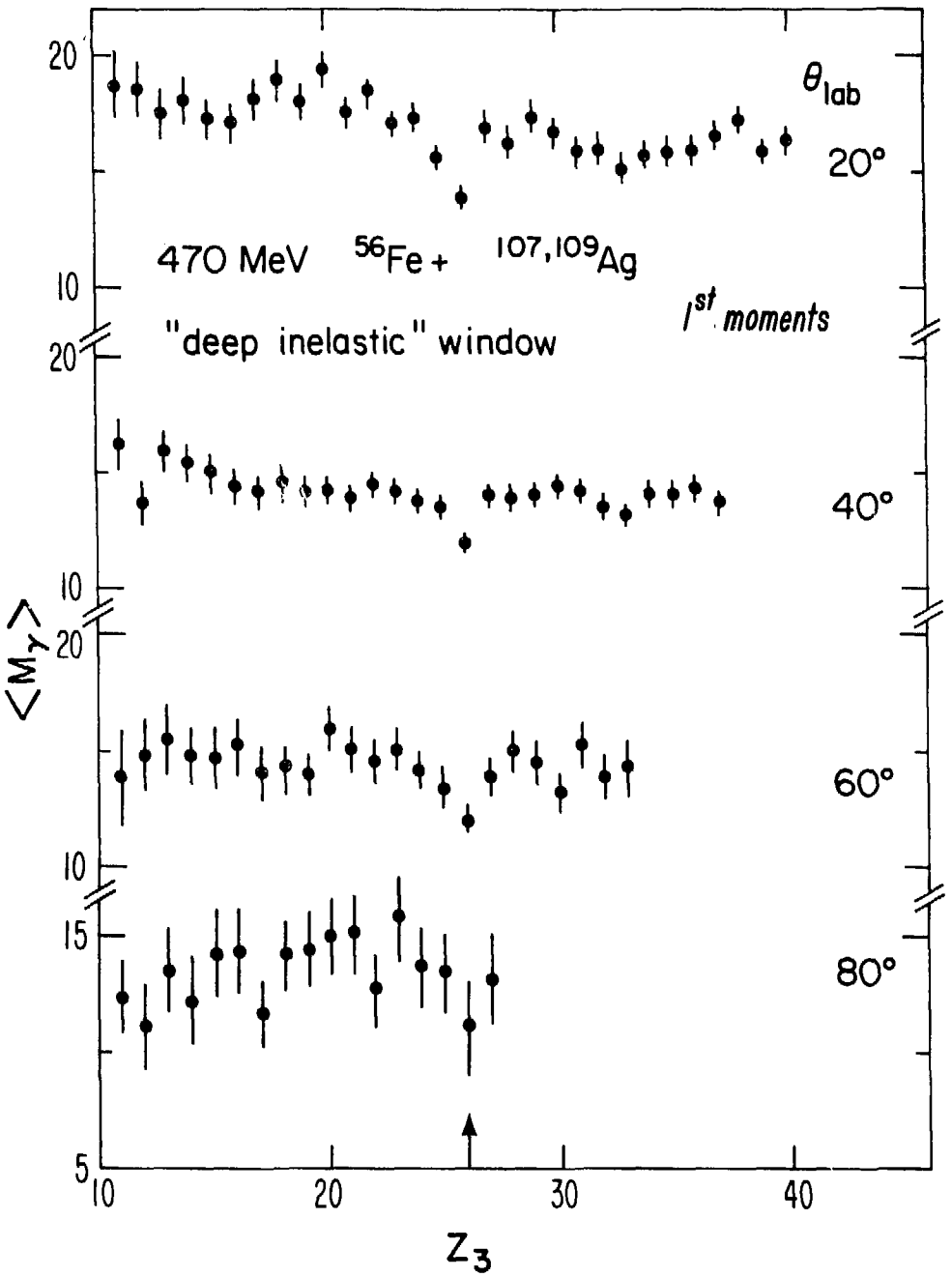

XBL 788-2647

Fig. 17b

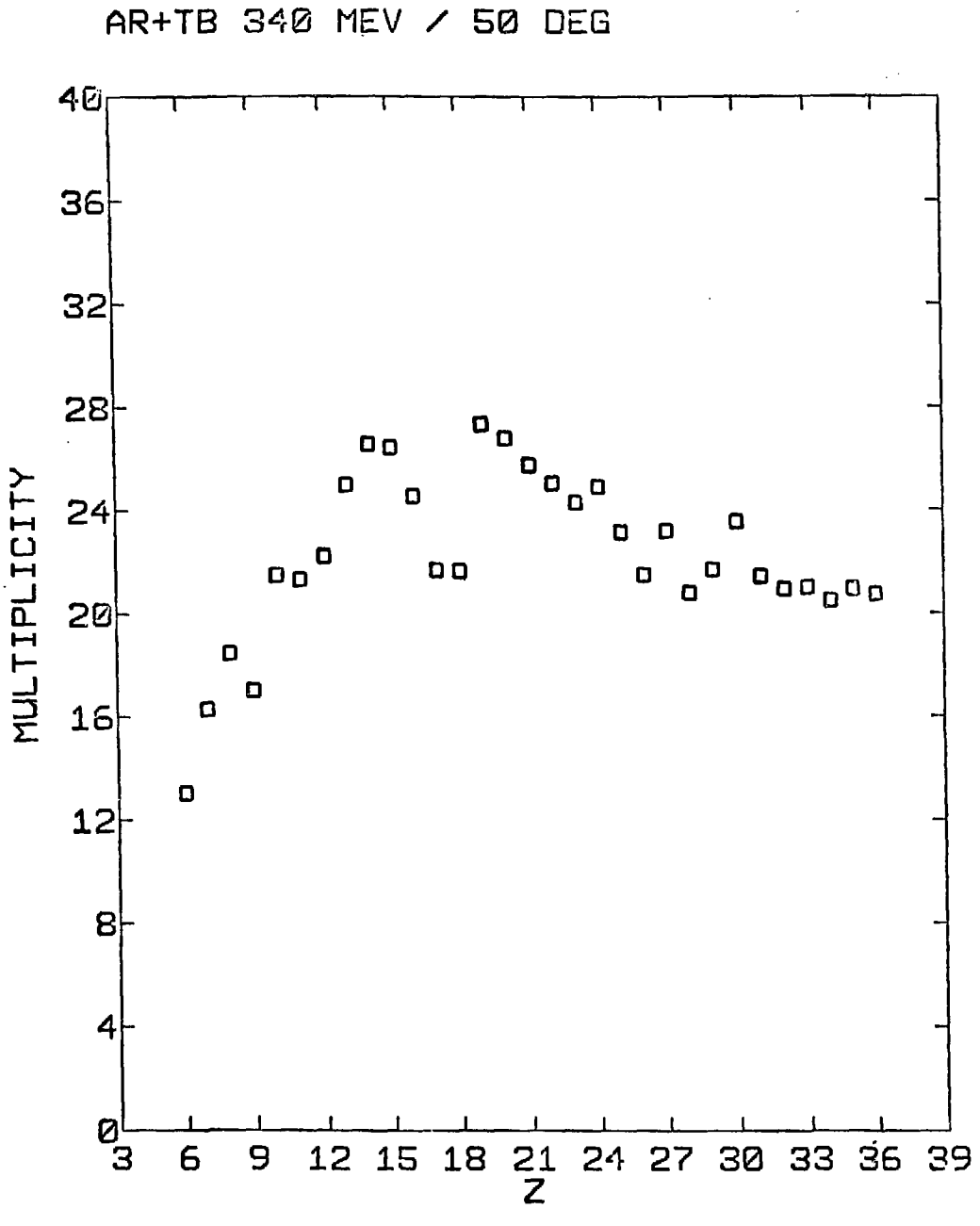

XBL 795-9880

Fig. 17c

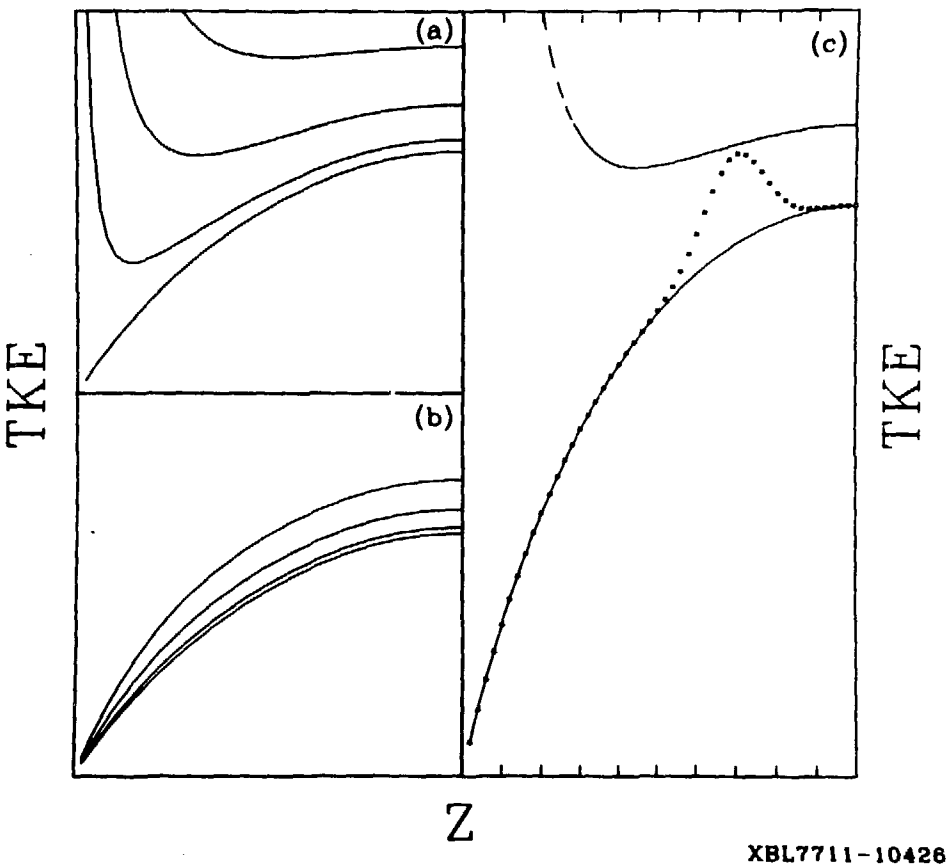

Fig. 18

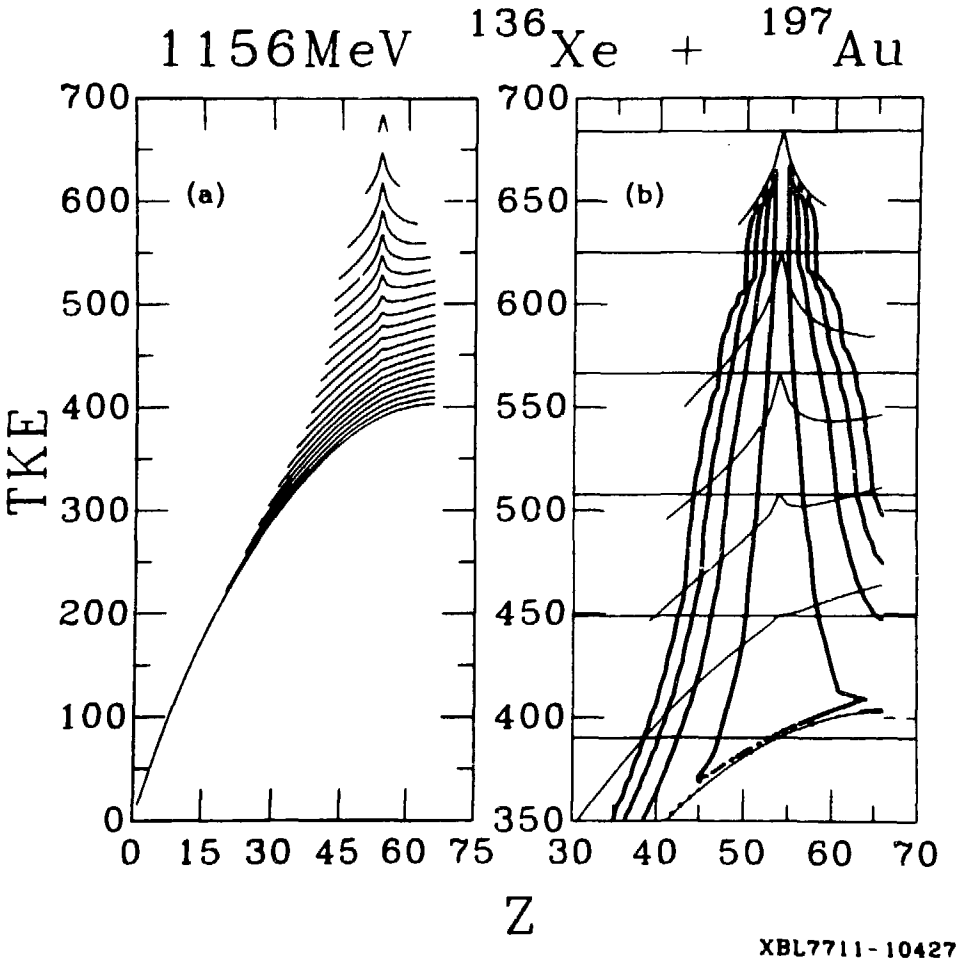
1156MeV ^{136}Xe + ^{197}Au
(a)
(b)
TKE
Z
700
600
500
400
300
200
100
0
0 15 30 45 60 75
700
650
600
550
500
450
400
350
30 40 50 60 70
XBL7711-10427

Fig. 19

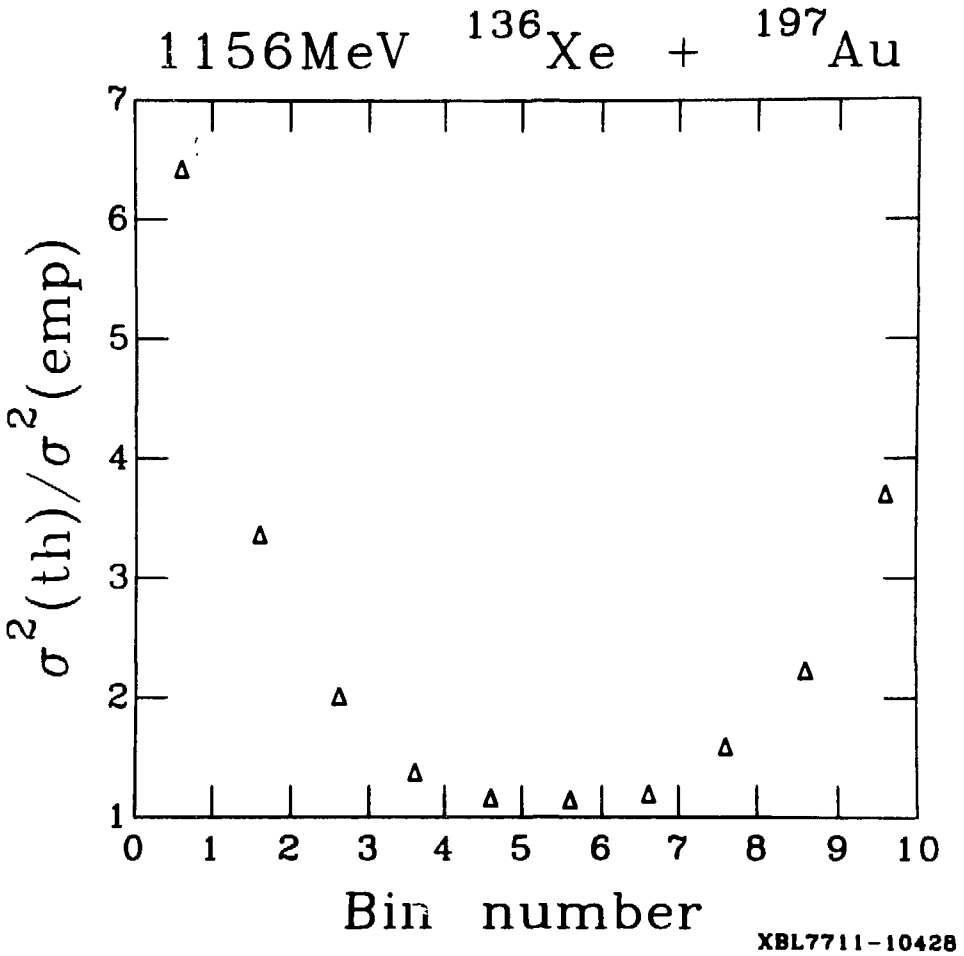
1156MeV ^{136}Xe + ^{197}Au
σ^2(th)/σ^2(emp)
Bin number
XBL7711-10428

Fig. 20

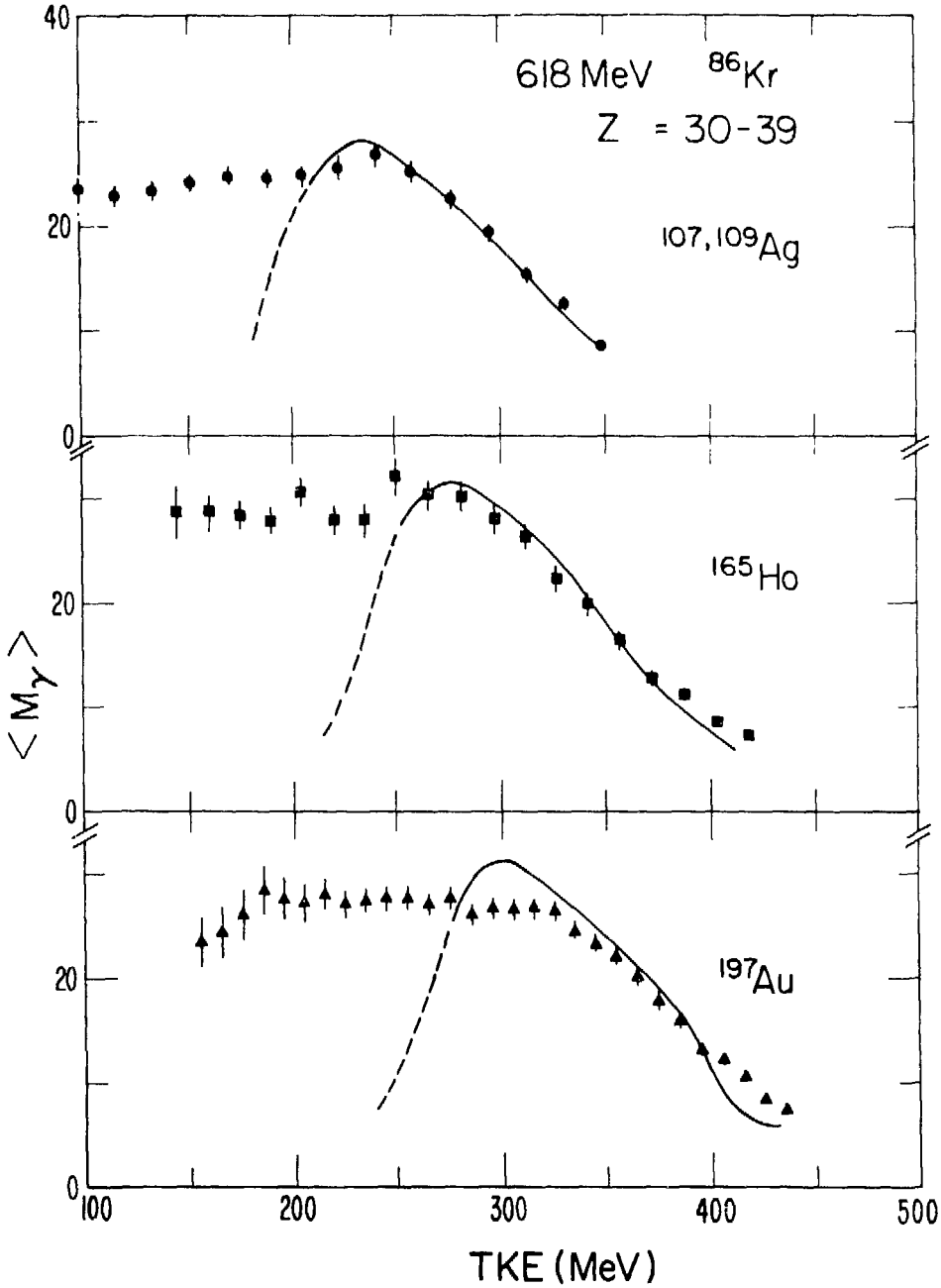

XBL 786-2553

Fig. 21

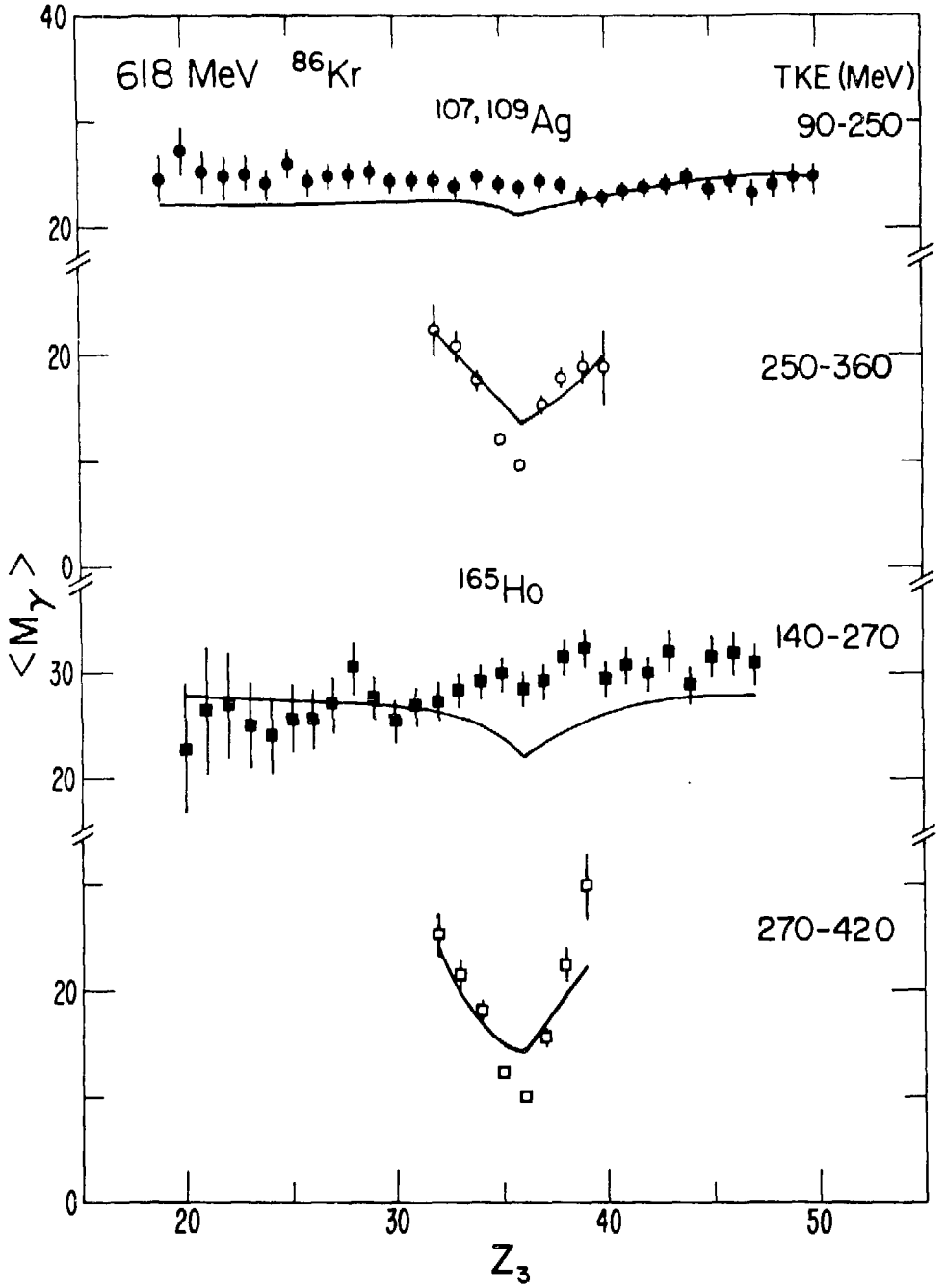

XBL 786-2556

Fig. 22

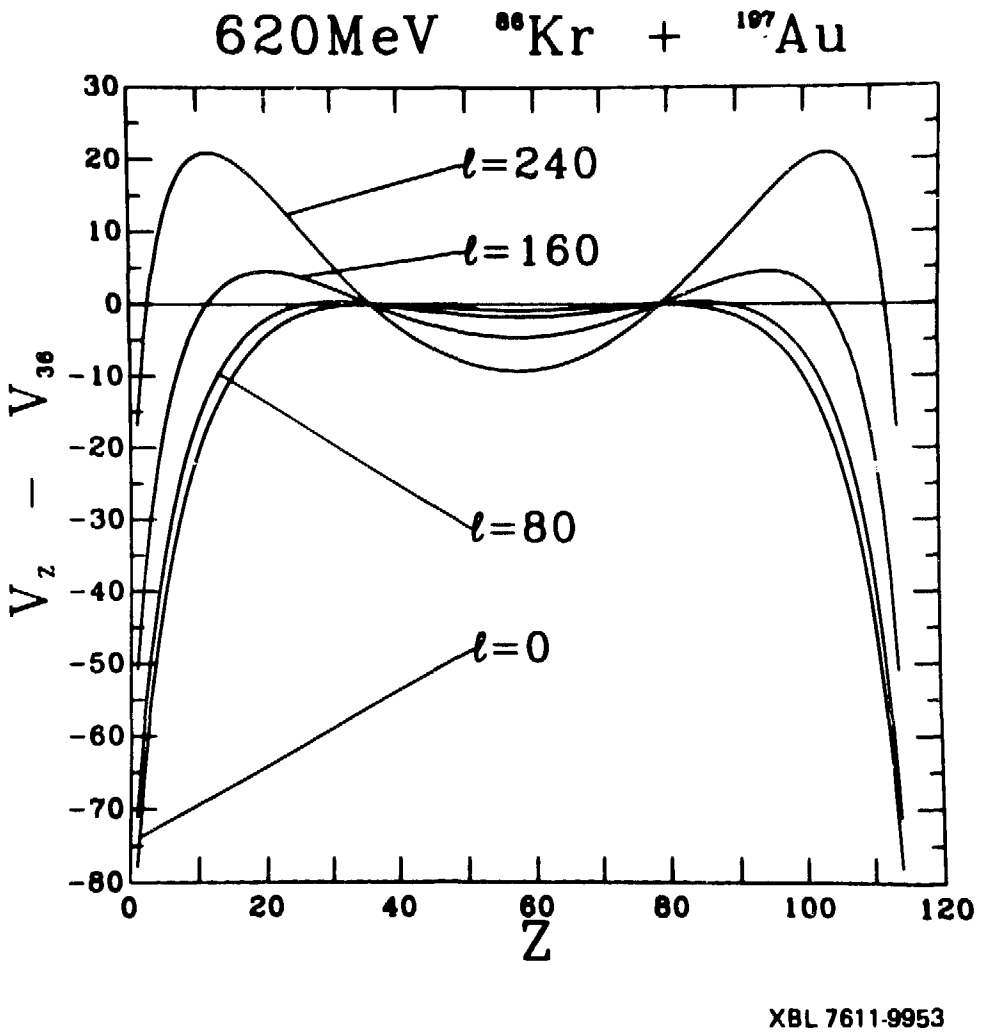

XBL 7611-9953

Fig. 23.

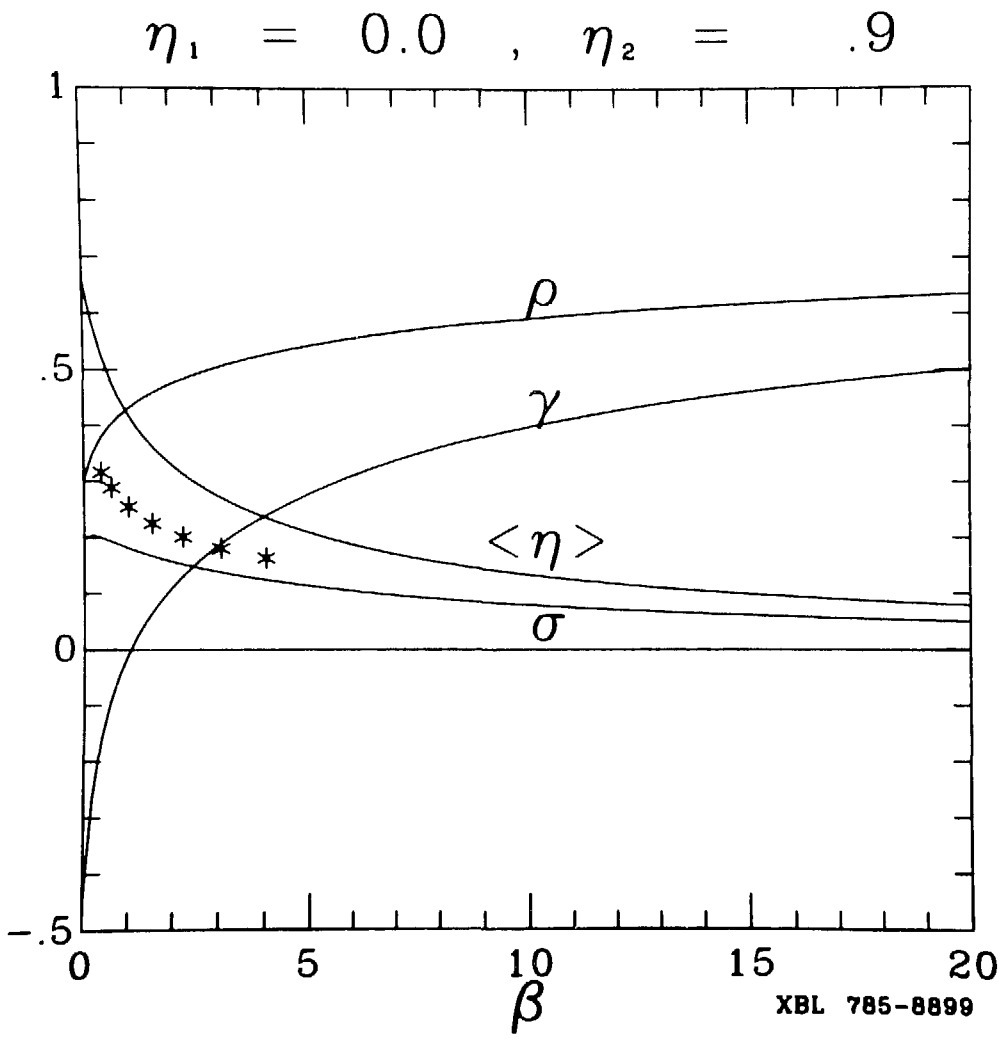
$\eta_1 = 0.0 , \eta_2 = .9$
1
.5
0
−.5
0
5
10
15
20
β
ρ
γ
$\langle\eta\rangle$
σ
XBL 785-8899

Fig. 24

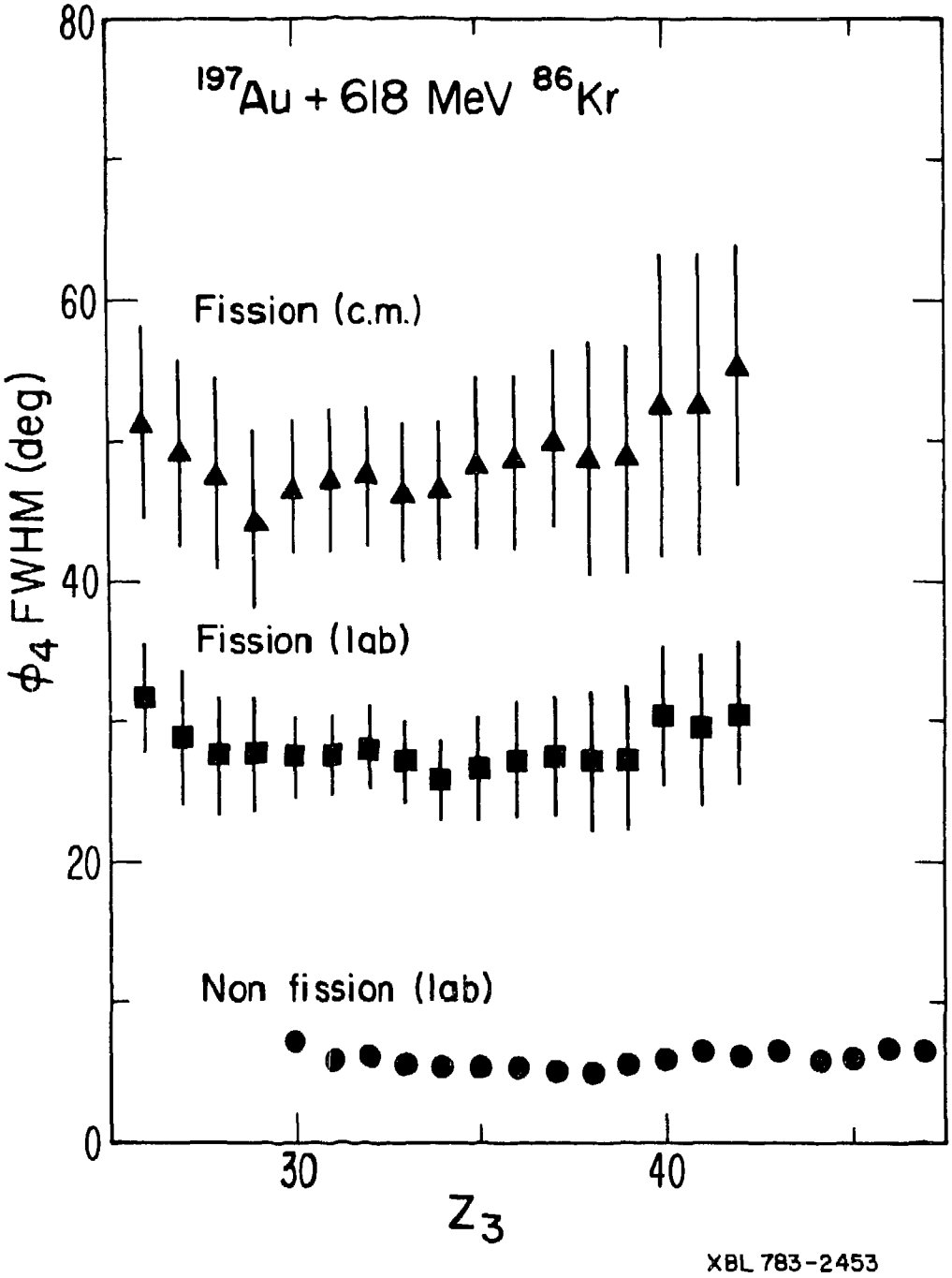
^{197}Au + 618 MeV ^{86}Kr
Fission (c.m.)
Fission (lab)
Non fission (lab)
ϕ_4 FWHM (deg)
80
60
40
20
0
30
40
Z_3
XBL 783-2453

Fig. 25